# Review of pressurized chemical looping processes for power generation and chemical production with integrated $CO_2$ capture

Mogahid Osman[a], Mohammed N. Khan[a,b], Abdelghafour Zaabout[c], Schalk Cloete[c], Shahriar Amini[d1]

[a]Norwegian University of Science and Technology, Department of Energy and Process Engineering, Trondheim, Norway
[b]Flemish Institute for Technological Research, Unit Separation and Conversion Technologies, Mol, Belgium
[c]SINTEF Industry, Process Technology Department
Trondheim, Norway
[d]Department of Mechanical Engineering, University of Alabama, Tuscaloosa, AL, U.S.A

## Abstract

Chemical looping has great potential for reducing the energy penalty and associated costs of $CO_2$ capture from fossil fuel-based power and chemical production while maintaining high efficiency. However, pressurized operation is a prerequisite for maximizing energy efficiency in most proposed chemical looping configurations, introducing significant complexities related to system design, operation and scale-up. Understanding the effects of pressurization on chemical looping systems is therefore important for realizing the expected cost reduction of $CO_2$ capture and speed up the industrial deployment of this promising class of technologies.

This paper reviews studies that investigated three key aspects associated with pressurized operation of chemical looping processes. First, the effect of pressure on the kinetics of the various reactions involved in these processes was discussed. Second, the different reactor configurations proposed for chemical looping were discussed in detail, focusing on their suitability for pressurized operation and highlighting potential technical challenges that may hinder successful operation and scale-up. Third, techno-economic assessment studies for these systems were reviewed, identifying the process configuration and integration options that maximize the energy efficiency and minimize the costs of $CO_2$ avoidance.

Prominent conclusions from the review include the following. First, the frequently reported negative effect of pressure on reaction kinetics appears to be overstated, implying that pressurization is an effective way to intensify chemical looping processes. Second, no clear winner could be identified from the six pressurized chemical looping reactor configurations

*Corresponding author: Dr. Shahriar Amini, SINTEF Industry, S.P. Andersens vei 15 B, 7031, Trondheim, Norway, Phone: +47 46639721, Email: shahriar.amini@sintef.no, samini3@ua.edu

reviewed. Further information on elements such as oxygen carrier durability, technical feasibility of downstream high-temperature valves and filters, and scale-up challenges will be required to select the best configuration. Third, the maximum reactor temperature imposes a major constraint for combined cycle power production applications, requiring an extra combustor after the reactor. Hydrogen production applications do not face such constraints and can approach the techno-economic performance of unabated benchmarks. Flexible power and hydrogen chemical looping plants appear promising for integrating renewable energy. Based on these findings, pressurized chemical looping remains a promising decarbonization pathway and further development is recommended.

*Keywords:*

*Chemical looping process; High pressure; $CO_2$ capture; Power production; Hydrogen production*

Contents:

## 1. Introduction

Greenhouse gas emissions from fossil fuel utilization can be reduced by several options that include i) improving the process efficiency, ii) switch to renewable energy sources, iii) replacement of coal by natural gas (containing less carbon content) and iv) applying Carbon Capture, Utilization and Storage (CCUS). According to the Intergovernmental Panel on Climate Change (IPCC), CCUS would play a major role in most mitigation scenarios to meet the global warming targets [1]. Four main categories have been explored for $CO_2$ capture technologies: 1) post-combustion, 2) pre-combustion, 3) oxy-combustion, and 4) chemical looping process [2]. For power production, the first three concepts incur a significant loss of efficiency and power output that has a large effect on the economics [3]. The chemical looping process is an alternative option that has the potential to intrinsically reduce the energy losses associated with $CO_2$ capture [4]. The chemical looping system carried is out in two steps; in the fuel reactor (FR) the fuel reacts with an oxygen carrier (metal oxide) to form $CO_2$ and $H_2O$; the reduced metal oxide is then circulated for re-oxidization in a flow of air in the air reactor (AR). The exothermic oxidation reaction in the AR produces heat that is utilized for power production [5–7]. Beyond power production, the chemical looping concept has been applied in the production of hydrogen [8–10], syngas [5,6,11] and oxygen [12,13]. Recent reviews on chemical looping process can be found in Adánez et al. [14], Mattisson et al. [15], Lyngfelt et al. [16], and Zhu et al. [17]. Fig. 1. shows an overview of the various technologies that utilize oxygen carriers in a chemical looping system.

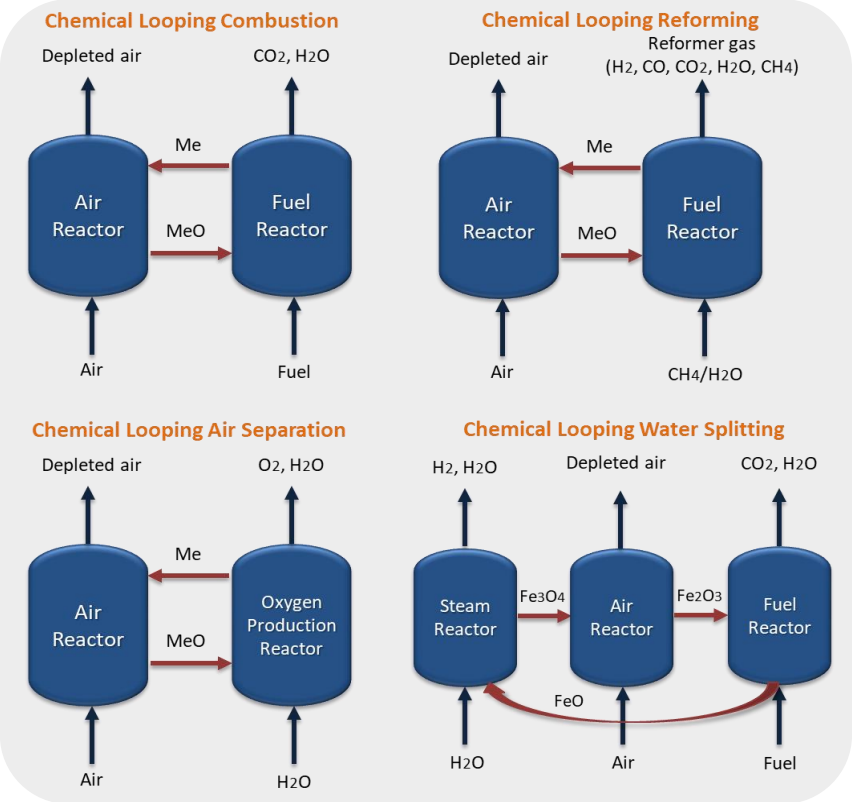


Fig. 1. Chemical looping process for different applications.

In power generation, pressurized chemical looping has the potential for maximizing the power plant efficiency by using a combined cycle instead of the Rankine cycle used with atmospheric pressure boilers. The pressurized hot depleted air from the AR is used to drive a gas turbine (Brayton Cycle) followed by a heat-recovery steam generator (HRSG) for additional power generation (Rankine Cycle). The $CO_2$ rich stream from the FR could also be expanded and used for heat recovery for additional power generation, followed by water condensation then $CO_2$ compression and sequestration. Moreover, high-pressure combustion increases the temperature at which the steam in the FR outlet stream condenses; hence, some of the heat of condensation can be utilized within the process, which increases the thermal energy recovery from the fuel (the higher heating value instead of the lower heating value). This is especially interesting for CLC with natural gas given the high moisture content in the FR flue gas (2 parts $H_2O$ and 1 part $CO_2$). The high temperature condensate can be utilized for preheating the water feed of the Rankine cycle, which reduces or eliminates the need of extracting part of the steam from the

cycle and hence increasing the efficiency of the system (steam extraction is inevitable in atmospheric combustion process to achieve target feed water temperature).

Other benefits for high-pressure CLC (PCLC) operation include reduced power consumption for $CO_2$ compression or refrigeration steps, and increased heat transfer rates. Thermodynamic investigations have revealed that the integration of PCLC with a natural gas fired combined cycle (NGCC) can achieve a power efficiency of 52 to 55% (LHV), which is higher than NGCC with post-combustion $CO_2$ capture by 3-5% points [18,19]. For hydrogen production, high-pressure operation improves the overall efficiency and lowers the cost associated with hydrogen separation and compression [20]. For syngas production, high-pressure operation is required for improving the efficiency of syngas to liquids processes [20]. Moreover, high-pressure operation significantly reduces the process footprint (increasing pressure reduces the gas volume), thus resulting in more compact reactors.

Considering these advantages, several experimental and modelling studies, reported in the literature, investigated pressurized chemical looping systems. While elevated pressures fundamentally have a positive influence on the overall plant efficiency, there are many contradictions in the literature on the effect of pressurized conditions on the overall performance of chemical looping systems. Pressurized operation influences the process performance in terms of reaction kinetics, heat and mass transfer rate, $CO_2$ capture efficiency, product selectivity and fuel conversion. Considering these parameters, experimental campaigns in the literature were carried out in various systems and configurations such as pressurized thermo-gravimetric analyzer (PTGA), fluidized-bed, fixed-bed and moving-bed systems. Likewise, modelling and simulation studies were carried out to gain insights into the effect of pressure on the behavior of several oxygen-carriers for chemical looping systems.

This paper aims to establish a comprehensive review of the research outcomes of pressurized chemical looping processes with emphasis on kinetics, reactor configurations, and techno-

economic studies. The different factors affecting the reaction kinetics in pressurized chemical looping are highlighted and the suitability of the various reactor configurations reported in the literature for pressurized operation is discussed based on their working principle and their level of advancement achieved to date.

## 2. Kinetic analysis

This section reviews studies conducted to reveal the effect of pressure on the kinetics of the reactions involved in the chemical looping systems. The section is divided into two sub-sections: oxygen carrier reactivity studies and kinetic models.

### 2.1. Oxygen carrier reactivity studies

In principle, there are three types of pressure effects on the reduction kinetics: 1) effect of total pressure at a constant fuel partial pressure, 2) effect of total pressure at a constant fuel molar fraction, and 3) effect of fuel partial pressure at a constant total pressure. The following three sub-sections classify and discuss the reported results based on the above-mentioned effects. The last section presents the results reported for the oxidation kinetics at pressurized conditions. Table 1 summarizes the various operating conditions used for studying oxygen carrier reactivity and kinetics under high pressure.

**Table 1. Summary of the experimental techniques and operating conditions used for oxygen carrier reactivity and kinetics studies under high pressure.**

| Reference | Oxygen-carrier/Fuel | Experimental conditions |
|---|---|---|
| García et al. (2006) [21] | **OC:**<br>$CuO/Al_2O_3$<br>$Fe_2O_3/Al_2O_3$<br>$NiO/Al_2O_3$<br><br>**Fuel**:<br>CO and $H_2$ | • 800°C<br>• P: 1 - 30 bar<br>**Type of Experiments:**<br>• Constant gas partial pressure of 1 bar and different total pressures |

| | | |
|---|---|---|
| Abad et al. (2007) [22] | **OC:**<br>$CuO/Al_2O_3$<br>$Fe_2O_3/Al_2O_3$<br>$NiO/Al_2O_3$<br><br>**Fuel:**<br>Syngas | • T: 550 - 950°C<br>• P: 1 and 20 bar<br>**Type of Experiments:**<br>• Two kinds of experiments: constant partial pressure and constant volume fraction of the fuel gas |
| Siriwardane et al. (2007) [23] | **OC:**<br>NiO/bentonite<br>**Fuel:**<br>Syngas | • T: 800°C<br>• P: 1, 3.5, 7 bar<br>**Type of Experiments:**<br>• Constant fraction of the fuel gas |
| Gu et al. (2013) [24] | **OC:**<br>Iron Ore<br>(Hematite, $Fe_2O_3$)<br><br>**Fuel:**<br>CO | • T: 800°C<br>• P: 1 and 6 bar<br>**Type of Experiments:**<br>• Constant volume fraction of the fuel gas |
| Zhang et al. (2014) [25] | **OC:**<br>Iron ore<br>(Hematite, $Fe_2O_3$)<br><br>**Fuel:**<br>Bituminous coal | • T: 950°C<br>• P: 1, 5 and 10 bar<br>• 18.9 % steam in $N_2$ used as gasifying agent<br>**Type of Experiments:**<br>• Constant fraction of the fuel gas |
| Luo et al. (2014) [26] | **OC:**<br>$Fe_2TiO_5$<br>Iron-titanium composite metal oxide (ITCMO)<br><br>**Fuel:**<br>$CH_4$ | • T: 950°C<br>• P: 1-10 bar<br>**Type of Experiments:**<br>• Constant mole fraction of the fuel gas |
| Hamers et al. (2015) [27] | **OC:**<br>$CuO/Al_2O_3$<br>$NiO/CaAl_2O_4$<br>**Fuel:**<br>CO<br>$H_2$ | • T: 550 - 950°C<br>• P: 1-20 bar<br>**Type of Experiments:**<br>• Two kinds of experiments: constant partial pressure of the fuel at 1 bar, constant gas mole fraction of the fuel at 20% |
| Deshpande et al. (2015) [28] | **OC:**<br>$Fe_2TiO_5$<br>Iron-titanium composite metal oxide (ITCMO)<br><br>**Fuel:**<br>$H_2$ | • T: 900°C<br>• P: 1-10 bar<br>**Type of Experiments:**<br>• Three kinds of experiments: 1) constant partial pressure, 2) constant mole fraction of the fuel gas, 3) constant total pressure with various partial pressure of the fuel |
| Lu et al. (2016) [29] | **OC:**<br>ilmenite ore<br>(titanium-iron oxide, $FeTiO_3$)<br>**Fuel:**<br>CO | • T: 950°C<br>• P: 16 and 24 bar<br>**Type of Experiments:**<br>• Two kinds of experiments: 1) constant partial pressure, 2) constant total pressure with various fuel partial pressure |
| San Pio et al. (2017) [30] | **OC:**<br>$CuO/Al_2O_3$<br>**Fuel:**<br>$H_2$ | • T: 800°C<br>• P: 1-10 bar<br>**Type of Experiments:**<br>• Two kinds of experiments: 1) constant partial pressure of $H_2$ and constant gas flowrate, 2) constant partial pressure of $H_2$ and increasing the gas flowrate with pressure |
| Tan et al. (2017) [31] | **OC:**<br>ilmenite ore<br>(titanium-iron oxide, $FeTiO_3$) | • T: 750 - 950°C<br>• P: 6, 9, 16 bar<br>**Type of Experiments:** |

| | | |
|---|---|---|
| | **Fuel:**<br>Natural gas | • Two kinds of experiments: 1) constant partial pressure, 2) constant total pressure with various fuel partial pressure |
| Tan et al. (2017) [32] | **OC:**<br>ilmenite ore<br>(titanium-iron oxide, $FeTiO_3$)<br>**Fuel:**<br>$CH_4$ | • T: 850 - 950°C<br>• P: 6-16 bar<br>**Type of Experiments:**<br>• Two kinds of experiments: 1) constant partial pressure, 2) constant total pressure with various fuel partial pressure |
| Chen et al. (2017) [33] | **OC:**<br>ilmenite ore (titanium-iron oxide, $FeTiO_3$)<br>Red mod (bauxite residue contains ~50% $Fe_2O_3$)<br>**Fuel:**<br>Coal char | • T: 950°C<br>• P: 1, 2, 4, 6 bar<br>**Type of Experiments:**<br>• Constant amount of solid-fuel and with increasing the gas flowrate linearly with pressure (constant superficial gas velocity).<br>• • Steam used as gasification agent. |
| Rana et al. (2019) [34] | **OC:**<br>ilmenite ore<br>(titanium-iron oxide, $FeTiO_3$)<br>**Oxidation agent:**<br>Air | • T: 800 - 1050°C<br>• P: 1-16 bar<br>**Type of Experiments:**<br>• Two kinds of experiments: 1) constant $O_2$ partial pressure, 2) constant total pressure with various $O_2$ partial pressure |
| Díez-Martín et al. (2018) [35] | **OC:**<br>CuO<br>**Oxidation agent:**<br>Air | • T: 850°C<br>• P: 1-10 bar<br>**Type of Experiments:**<br>• Constant $O_2$ concentration |

### 2.1.1. Constant fuel partial pressure

Experimental studies conducted at constant fuel partial pressure while increasing the total pressure by dilution with inert gas revealed a contradicting effect of the pressure on the reduction rates for all oxygen carriers and fuels studied. For instance, García et al. [21] conducted a kinetics investigation using a pressurized thermogravimetric analysis (PTGA) for different oxygen carriers based on Cu, Fe and Ni in a pressure range of 1 to 30 bar. The reduction rates were found to decrease with increasing the total pressure. It was reported that the reaction rate was highly affected by the gas dispersion of the system, especially during the initial stage of introducing the reacting gas to the sample cell. It should be noted that, the term “gas dispersion” used by the authors of this study and on the following studies is most properly referred to as "the external mass transfer resistance", i.e. the finite rate of reacting species transport to the outer surface of the particles. The work of Lu et al. [29] showed that the reduction of ilmenite ore (a titanium-iron oxide, $FeTiO_3$) with CO at constant partial pressure

and increasing the total pressure (by increasing $CO_2$ partial pressure) revealed a negative effect of pressure. They attributed this result to the increase of $CO_2$ partial pressure along with the total pressure, which from a thermodynamic point of view has a negative effect on the reduction rate. Tan et al. [31,32] extended the kinetic study of ilmenite ore with $CH_4$ and simulated natural gas as fuel (simulated natural gas is a gas mixture similar to the natural gas composition). The results showed that increasing the total pressure at constant fuel feed and $CO_2$ partial pressure reduced the reduction rate of the ilmenite ore. Increasing the temperature reduced the negative impact of the total pressure during the reduction phase. Tan et al. [31,32] explanation to the adverse effect of the total pressure was that increasing total pressure slowed down the product gas diffusion away from the gas-solid interface, and hence reduced the reactant gas ability to reach the active sites.

Hamers et al. [27] revealed the same phenomenon in the reduction kinetics of Cu and Ni based oxygen carriers at operating pressures up to 20 bar, which was attributed to the competitive adsorption of the inert gas with the reactive gases on the oxygen carrier surface. With higher inert dilution, larger space of the cavities was being blocked reducing the reaction rate. This effect becomes more pronounced at higher total pressure which is translated by the observed higher fluctuations in the experimental transient solids conversion at higher pressures (Fig. 2.a). This is in line with the observations in the works of García et al. [21] and Lu et al. [29].

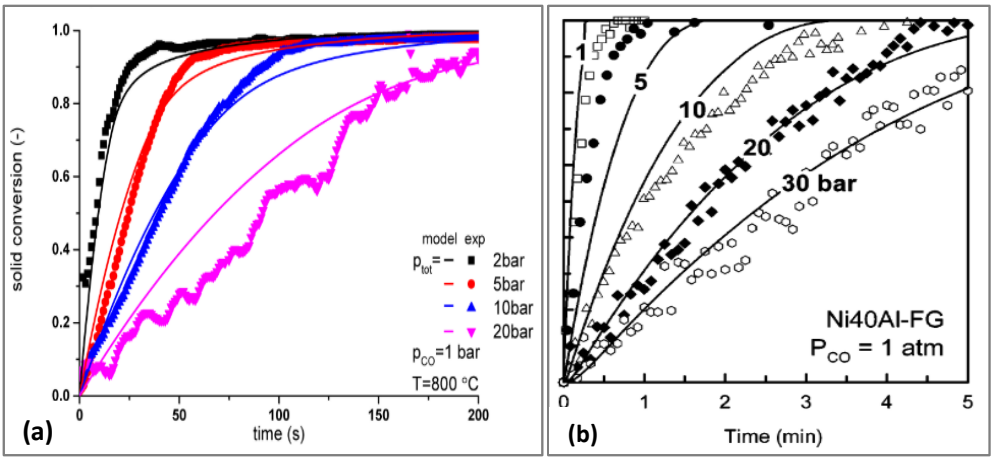

Fig. 2. Effect of the total pressure on the reduction kinetics of Ni-based oxygen carriers at a constant fuel partial pressure (1 bar) at 800°C. The markers show the experimental data, and the lines show the model predictions. a) [27] "Adapted with permission, Copyright (2015) ACS ", b) [21] "Adapted with permission, Copyright (2006) ACS ".

To minimize the effect of the gas dispersion (external mass transfer resistance) with elevated pressures; Deshpande et al. [28] used a constant gas space velocity in a reduction study of an ilmenite-based oxygen carrier. They showed an increase in the reduction rate with increasing the total pressure, thus counteracting the negative impact of gas dispersion in the unit cell that occurs when the flowrate was maintained constant. The work of San Pio et al. [30] supported this finding as shown in Fig. 3, showing that increasing the molar flowrate with the total pressure counteracted the negative effect of pressure on the reduction kinetics. This study was conducted using a Cu-based oxygen carrier and $H_2$ as fuel in a pressure range of 1 to 10 bar. Looking through these results (Fig. 3), it can clearly be seen that the external mass transfer resistance negatively affects the reduction kinetics and should partially be avoided by increasing the total molar flowrate with increasing the total pressure.

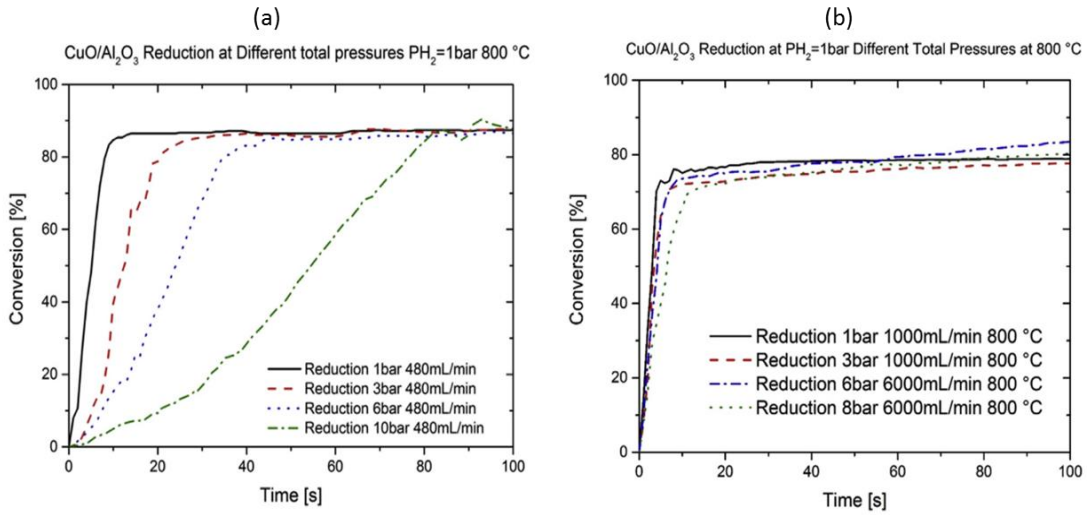


Fig. 3. Reduction conversions with different total pressure and constant fuel partial pressure at 800°C, a) at constant molar flowrate, b) at different molar flowrate [30], "Adapted with permission, Copyright (2017) Elsevier BV".

Similar results of the negative effects of total pressure on the reduction kinetic have been also reported in other non-catalytic gas-solid reactions; for example, for the capture of $H_2S$ and $CO_2$

by calcium-based sorbents [36–42], and the coal gasification process [43,44]. Although no consistent explanations were proposed for the negative effects of pressure, there was a common explanation that the intra-particle diffusion was hindered with increasing total pressure. The gas diffusivity coefficient combines both the molecular and Knudsen diffusivities. The molecular diffusivity is inversely proportional to the system pressure; however, the Knudsen diffusivity is independent of pressure as it depends only on the structure of the pore network. Therefore, increasing total pressure decreases the molecular diffusivity, which leads to a decrease in the effective gas diffusivity that could lead to the decrease in the overall conversion rate [45].

The external mass-transfer resistance could also be the main reason for the negative effect of the total pressure in all these studies; given that the authors used a constant gas flowrate among all pressurized kinetic tests. Increasing the total pressure of the system lowers the volumetric and superficial velocities of the gas; this will increase the time required for the gas to diffuse through the boundary layer to the particle surface, which would result in increased external mass-transfer resistance. By using higher superficial velocity, the boundary layer thickness decreases and therefore the film diffusion will no longer be a limiting step, and the observed reaction rate approaches the intrinsic reaction rate. Hecker et al. [44] studied the kinetic of char oxidation at high total pressure and constant $O_2$ partial pressure while increasing the total flowrate with pressure. They reported that the intrinsic char oxidation rate, activation energy, and oxygen reaction order were found to be independent of the total pressure implying that maintaining the superficial gas velocity constant had successfully reduced the negative effect of the external mass transfer on the observed reaction rates. A positive effect of pressure was reported by Butler et al. [46] for the kinetic of $CO_2$ carbonation using un-diluted $CO_2$ in a pressure range of 5 to 20 bar. Increasing the carbonation pressure was found to increase the carbonation rate and the calcium utilization over 100 cycles.

The reactant gas flowrate is not the only parameter that affects the intrinsic reaction rate but also other factors such as the solid weight, the solid holder geometry and the solid-particle dispersion [47]. In order to obtain a reliable kinetic parameters, all these factors should be optimized during the kinetics experiment to isolate any physical effect on the reaction kinetic. Kibria et al, [48] proposed a systematic experimental procedure to minimize the effects of the rate-influencing factors during $CO_2$ gasification of biomass char. Their strategy involves testing the effects of all the rate-limiting factors during TGA experiments and optimize the experimental conditions accordingly. Fig. 4 shows the results of the gasification rate for the changes in the various factors and the optimized condition, which revealed the highest reaction rate as it was free from all heat and mass transfer limitations. Pressurized gas-solids reaction kinetics exhibits more intrusion of the transport effects in the reaction rate measurement; therefore, a careful consideration of all physical factors is highly recommended for future kinetics studies to ensure accurate design and operation of the large-scale reactor.

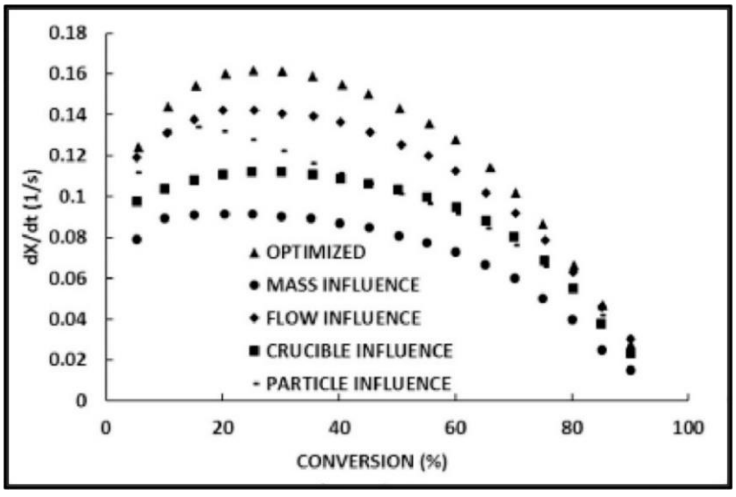


Fig. 4. The reaction rate during $CO_2$ gasification of biomass char for various rate-influencing factors and the optimized condition (triangle) [48], "Adapted with permission, Copyright (2019) Elsevier BV".

Fewer studies were reported for the kinetic of solid-fuel chemical looping combustion/gasification at elevated pressure [25,33,49]. In a typical coal-based CLC system,

the reactions between coal, oxygen carrier and the gasification agent ($H_2O$ or $CO_2$) occurs as a results of various reactions as following:

| | |
|---|---|
| $\text{Coal} \rightarrow \text{Char} + \text{Volatiles}$ | (1) |
| $\text{Char} + H_2O \rightarrow CO + H_2$ | (2) |
| $\text{Char} + CO_2 \rightarrow 2CO$ | (3) |
| $CO + H_2O \rightarrow CO_2 + H_2$ | (4) |
| $H_2 + \text{Metal Oxide} \rightarrow \text{Reduced Metal Oxide} + H_2O$ | (5) |
| $CO + \text{Metal Oxide} \rightarrow \text{Reduced Metal Oxide} + CO_2$ | (6) |

Coal pyrolysis (Equ.(1)) is the first stage of the CLC process, followed by char gasification (Equ.(2),(3)). The rate of char gasification is much slower than that of coal pyrolysis. The WGSR (Equ.(4)) catalyzed by the OC, also affects the composition of the final gaseous products. The presence of the OC primarily improves the gas phase conversion for complete oxidation of the combustible gases (Equ.(5),(6)); thus reducing hydrogen inhibition effect on char gasification and ultimately promoting char conversion further. Effects of pressure on the rate of coal CLC reactions is affected by the two stages (coal pyrolysis and char gasification) and the interaction of mass transfer and reaction of gas-solid and solid-solid phases.

Zhang et al, [25] carried out kinetic investigation of coal chemical looping combustion using a pressurized TGA. Iron ore was used as oxygen carrier at a reaction pressure of 1, 5 and 10 bar. Their results showed that the reaction rate decreased with increasing pressure in the initial coal pyrolysis stage, however, in the subsequent char gasification stage, the reaction rate was found to improve at higher pressure. The overall reaction rate was found to be increasing with increasing the pressure up to 5 bar then decreased at 10 bar, which was attributed to the negative effect of pressure on the coal pyrolysis stage [25]. Chen et al, [33] studied the effects of pressure on the reactivity of ilmenite and red mud OCs (red mud is a bauxite residue contains ~50%

$Fe_2O_3$) on char gasification reactions using a fluidized-bed system. Fig. 5 showed the effect of pressure on the gasification rate for the various OCs and without the OCs. For all cases, increasing pressure in the range of 1 to 6 bar led to increasing the char gasification rate. The red mud OC (line-2 in Fig. 5) improves the gasification rate by about 140-190% compared to conventional steam gasification without OC (line-1 in Fig. 5). The promotion effect of the red mud OC is due to its catalytic functionality and to the rapid consumption of syngas, hence decreasing the inhibition effects of syngas on char gasification. Similar results were reported by Guo et al. [49] for char gasification using $Fe_2O_3/Al_2O_3$ as OC in a pressure range of 1 to 12 bar.

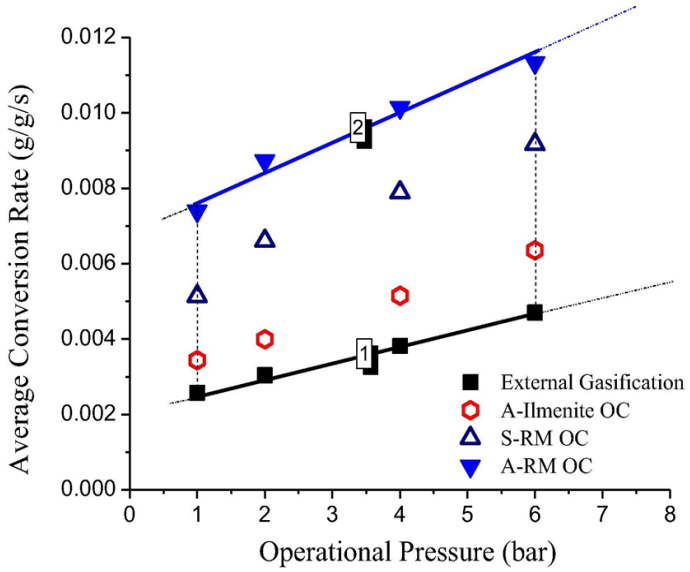


Fig. 5. The average gasification rate of PCLC and external gasification at various pressures [33], "Adapted with permission, Copyright (2017) Elsevier BV".

### 2.1.2. Constant fuel molar fraction

Increasing the total pressure while keeping the fuel molar fraction constant, would improve the reduction rate (due to increased fuel partial pressure). However, reduction kinetic studies revealed contradicting effects on the reaction rates among different studies. García et al. [21] showed a slight decrease in the reduction rate with increasing the total pressure up to 30 bar

while keeping the molar fraction of the fuel constant at 10%. They stated that various parameters affected the experimental results simultaneously including, gas dispersion, total pressure and partial pressure. Similar result was obtained by Hamers et al. [27] which was attributed to the decrease of the oxygen vacancies at higher pressures.

Positive effects of the pressure on the reduction kinetic were shown by Siriwardane et al. [23] using NiO based oxygen carrier supported on bentonite (bentonite is an aluminum phyllosilicate clay) for CLC with simulated syngas (12% $CO_2$, 36% CO, 25% He, and 27% $H_2$). Increasing the total pressure while keeping the reacting gas molar fraction constant showed an increase in the reduction rate, which was more significant at higher solid conversion. The positive effect of pressure at constant fuel molar fraction on the reduction rate is consistent with the work of Luo et al. [26] and Deshpande et al. [28] on the reduction kinetics of iron-titanium composite oxygen carrier ($Fe_2TiO_5$) with $H_2$ and $CH_4$. At a constant fuel molar fraction of 50%, the reduction rate with $H_2$ was doubled when increasing the pressure from 1 to 10 bar, while $CH_4$ reduction rate increased by 5 time the atmospheric reduction rate. The increase of the reduction rate with pressure was due to the use of constant space velocity for all pressures, which decreased the extent of the negative effect of gas dispersion with increasing the pressure [26,28]. Another conclusion shown in the works of Luo et al. [26] and Deshpande et al. [28] was that the reduction of $Fe_2TiO_5$ with $CH_4$ followed three distinct stages with respect to the reduction rate, resulting in a sinusoidal reaction conversion curve as a function of time [26,28]. Higher operating pressure resulted in early occurrence of carbon deposition (at lower solid conversion), which was consistent with the thermodynamic analysis. Fig. 6. shows the reduction conversion curve obtained using $CH_4$ between 1 and 10 bar, where the three distinct reduction stages can clearly be identified. After analyzing this result with calculating the reduction rate for each stage, Deshpande et al. [28] have shown that a plateau in the reduction rate of stage I and III was found (Fig. 6. ), while an exponential increase of the reduction rate

was found for stage II [28]. The overall reduction rate was mostly affected by stage II reduction rate which is the slowest stage (the rate determining step) [28].

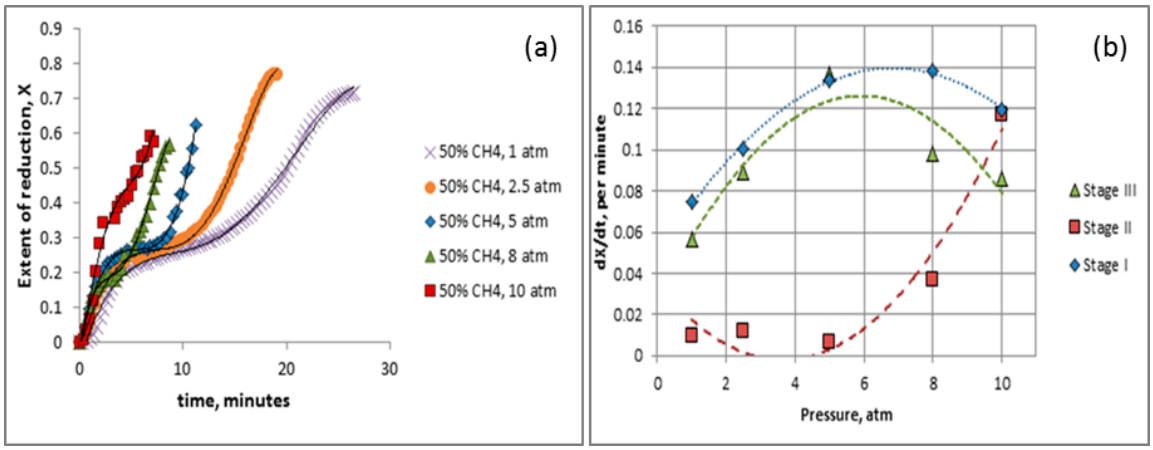


Fig. 6. Effect of the total pressure on the reduction kinetics of iron-based oxygen carriers with a constant fuel mole fraction ($CH_4$=50%) at 950°C, a) the reduction conversions, b) the reaction rate for the three-step reduction [28], "Adapted with permission, Copyright (2015) ACS".

### 2.1.3. Constant total pressure

Conducting oxygen carrier reduction at constant total pressure while increasing the fuel partial pressure increases the fuel concentration and hence increases the contribution of the gas phase to the overall reaction rate, and thus higher solid reduction rates are expected. Deshpande et al. [28] demonstrated this positive effect using $H_2$ as fuel and iron-titanium composite as oxygen carrier. The work of Luo et al. [26] and Tan et al. [31,32] also revealed the same conclusion using ilmenite ore and CO, $CH_4$ and simulated natural gas as fuel (simulated natural gas is a gas mixture similar to the natural gas composition). They found that increasing the fuel partial pressure while keeping the same fuel/$CO_2$ ratio and total pressure boosted the ilmenite reduction rate. However, the oxygen carrying capacity decreased with increasing the fuel partial pressure, especially at higher temperature. The authors attributed this negative effect to the fast reaction rate at high partial pressure that may have caused coverage of the oxygen carrier surface that hindered further reaction to happen. The faster the reaction rate, more of the OC active sites will be covered quickly and hence the product gas diffusion become slower,

controlling the reaction process, which hinders further reactions. With higher temperature, the involved reactions proceed even faster so this effect became more pronounced.

### 2.1.4. High pressure oxidation kinetics

Fewer studies were conducted for the oxidation kinetics at high pressure. Rana et al. [34] reported oxidation kinetics of a natural ilmenite ore at a temperature of 900°C and a pressure range of 1 to 16 bar. The results showed a negative effect of pressure on the oxidation rate when keeping the $O_2$ partial pressure constant. The authors did not provide an explanation for this effect; however, a possible explanation could be that the gas flowrate was not high enough to overcome the increased mass transfer resistance with pressure. When keeping the $O_2$ molar fraction constant, Rana et al. [34] revealed a positive effect on increasing the total pressure up to 8 bar, above which increasing the pressure had a negligible effect on the oxidation rate. Díez-Martín et al. [35] revealed a similar result for the oxidation kinetics of a CuO-based OC, in which increasing the total pressure (1 to 10 bar) while fixing the $O_2$ molar fraction resulted in a slight increase in the oxidation rate.

## 2.2. Kinetic Models

In this section, the kinetic models reported for high-pressure redox reactions are presented and discussed. The fuel reaction with the oxygen carrier is considered as a non-catalytic gas-solid reaction and the design and performance of the chemical looping reactors are strongly dependent on the kinetics of these reactions. Therefore, a kinetic model able to accurately predict the overall reaction rate is essential for successful chemical looping process design. To estimate the kinetic parameters, two approaches were followed in the literature for the inclusion of the pressure effects on the kinetic model of the redox reactions. One approach is by incorporating an empirical fitting parameter for the pressure to a kinetic model developed based on data conducted at atmospheric conditions [21,27,50]. The second is by developing the

kinetic model based on pressurized experiments [29,31,32]. The second one is the most accurate approach to capture the effects of pressure in a kinetic model that can be utilized for design and optimization of the larger scale process. Table 2. summarizes the different kinetic models and kinetic parameters reported by different studies on pressurized chemical looping process.

García et al. [21] applied the changing grain size model (CGSM) to the reduction reactions of Cu-, Ni- and Fe- based oxygen carriers. They considered two different grain geometries based on the structural differences and the preparation methods of the oxygen carriers. CuO-based OC prepared by impregnation method while Fe- and Ni-based OC prepared by freeze-granulation method. A SEM-EDX analysis of the three OC showed that Fe- and Ni-based OC had a granular structure while the Cu-based OC appears to be well-dispersed in the porous surface of the support structure. Accordingly, a spherical grain was considered for Fe- and Ni-based oxygen carriers, while a plate-like geometry was considered for the CuO-based oxygen carrier. The CGSM assumes that a number of uniform grains form the solids particles and it individually reacts based on a shrinking core model. The grain size changes as the reaction progresses, while the unreacted core shrinks. In their study, the kinetic parameters were obtained based on atmospheric pressure experiments, while an empirical parameter was used to fit the experiments conducted at higher pressure. The equations that describe the CGSM are shown in Table 2. , where the kinetic constant follows the temperature-dependence Arrhenius equation as follow:

$$k = k_0\, e^{-E/RT} \tag{7}$$

The apparent pre-exponential factor was estimated based on the total pressure and the pre-exponential factor obtained at atmospheric pressure as in Equ. (8) below:

$$k_{0,p} = \frac{k_0}{P^d} \quad (8)$$

Various kinetic parameters were obtained depending on the reaction and oxygen carrier considered, the resulted activation energy and reaction order are listed in Table 2.

The changing grain size model (CGSM) was also used by Lu et al. [29] for the reduction of the ilmenite ore with CO. In this study, they applied the model to data obtained at high pressure (16 bar). The reduction rate was accurately captured by the model for conversions below 70%. The activation energy and the reaction order values are listed in Table 2. Hamers et al. [27] developed a particle model with considering reaction kinetics, molecular diffusion, and Knudsen diffusion to capture the reduction rate inside the OC particles (NiO-based OC). They followed the same approach of García et al. [21] by extracting the kinetics parameters using experiments conducted at atmospheric pressure and by applying fitted parameters for the pressurized experiments. The OC particles used have a particle size of 1.1 mm, which is suitable for packed-bed chemical looping reactor configuration (to maintain a low pressure drop over the reactor). Using a large OC particle could impose a significant influence on the internal diffusion limitations that could lead to decreasing the effective reaction rates. However, the results of Hamers et al. [27] showed that increasing the pressure led to decreasing the effects of the diffusion limitations, which was attributed to the decrease in the reaction rates and the increase in the diffusion fluxes caused by Knudsen diffusion.

Tan et al. [31,32] adopted a kinetic model based on a phase-boundary-controlled mechanism with a contracting sphere for the reduction of ilmenite ore with methane and simulated natural gas. Tan et al. [31,32] used TGA experiments conducted at 9 and 16 bar to estimate the kinetic parameters. Table 2. listed the resulted activation energies at 9 and 16 bar. The model was able to capture the experimental results for a conversion ratio up to 70%.

Zhang et al. [50] described the reduction rate of iron-based oxygen carrier with CO as fuel considering an adapted random pore model (as shown in Table 2. ). The random pore model avoids the assumption of the grain model of constant grain and shape factors that in reality change in size during the reaction. The model incorporates the pore size distribution, pore growth and coalescence, which affects the diffusion inside the pores and surface area for reaction, all of which can be related to the initial properties of the oxygen carrier particles undergoing the reaction. These properties determine whether the overall reaction is reaction controlled or reaction-diffusion controlled or a combination of these as described by Everson et al. [51]. The model also incorporates several resistances that might be the reduction rate limiting steps, including external mass transfer, intra-particle diffusion, product layer diffusion, and chemical reaction. The model was developed using experiments carried out at atmospheric pressure and applied to the pressurized reaction kinetics up to 5 bar. The model indicated that the reduction of $Fe_2O_3/Al_2O_3$ exhibits a surface reaction controlled mechanism. The reaction order for surface reaction was close to 1 at 3 bar. The activation energy for the $Fe_2O_3/Al_2O_3$ were found to be (102 $kJ.mol^{-1}$) higher than those for the pure $Fe_2O_3$ oxygen carrier particles (61 $kJ.mol^{-1}$) and was attributed to the effect of $Al_2O_3$ support material on the reaction mechanism [50]. The presence of $Al_2O_3$ support improves the product layer diffusivity and hence enhances solid state diffusion facilitating the interaction of the active solid surface to the reducing gas [50].

**Table 2. Summary of the different kinetic models and kinetic parameters reported by different studies on pressurized chemical looping**

| References | Experimental conditions | Kinetics Model | Kinetic Parameters |
|---|---|---|---|
| García et al. (2006) [21] | ▪ OC: Cu, Fe and Ni based<br>▪ Fuel: CO and $H_2$<br>▪ Pressure: 1 - 30 bar<br>▪ Kinetic parameters obtained at atmospheric pressure<br>▪ Fitted parameter (d) used for pressurized experiments | The changing grain size model (CGSM) under chemical reaction rate control.<br><br>Spherical grains:<br>$\frac{t}{\tau} = 1 - (1 - X)^{1/3} \qquad \tau = \frac{\rho_m r}{bk(C^n - C_{eq}{}^n)}$<br><br>Plate-like geometry:<br>$\frac{t}{\tau} = X \qquad \tau = \frac{\rho_m L}{bkC^n} \qquad k_{0,p} = \frac{k_0}{P^d}$ | Reduction:<br>$k_0 = 5.9 \times 10^{-6}$ - $2.3 \times 10^{-3}$<br>E = 14 – 33 kJ.mol$^{-1}$<br>n = 0.5 – 1.0<br>d = 0.47 – 1.03<br>Oxidation:<br>$k_0 = 4.7 \times 10^{-6}$ – $1.8 \times 10^{-3}$<br>E = 7 – 15 kJ.mol$^{-1}$<br>n = 0.2 – 1.0<br>d = 0.46 – 0.84 |
| Lu et al. (2016) [29] | ▪ OC: ilmenite ore<br>▪ Fuel: CO.<br>▪ Total Pressure: 16 bar<br>▪ $P_{CO}$: 3.2 - 8.0 bar<br>▪ Temperature: 850 - 1050°C | The changing grain size model<br>$\frac{t}{\tau} = 1 - (1 - X)^{1/3}$<br>$\tau = \frac{\rho_m r_g}{bk_s P_G^n}$ | Reduction:<br>$k_0 = 2.46 \times 10^{-2}$ (mol m$^{-2}$ Pa$^{-n}$ s$^{-1}$)<br>E = 115 kJ.mol$^{-1}$<br>n = 0.67 |
| Hamers et al. (2015) [27] | ▪ OC: NiO and CuO.<br>▪ Fuel: CO.<br>▪ Pressure: 1 - 20 bar<br>▪ Kinetic parameters obtained at atmospheric pressure<br>▪ Fitted parameter (d) used for pressurized experiments | copper: $r_i = \varepsilon_{g,p} k_0 \exp\left[\frac{-E_{act}}{R \cdot T}\right] C_g^n \left(\frac{p_{tot}}{10^5}\right)^{-q}$<br><br>nickel: $r_i = \frac{\varepsilon_{s,p} \rho_s \omega_{act}^0}{b \cdot M_j} \frac{dX}{dt} \qquad \frac{dX}{dt} = \frac{\frac{3C_g^n}{b \cdot r_0 \cdot C_s}}{\left(\frac{1}{k}(1-X)^{-\frac{2}{3}} + \frac{r_0}{D}(1-X)^{-\frac{1}{3}} - \frac{r_0}{D}\right)}$ | Reduction:<br>n = 0.6 – 0.8<br>d = 0.47 – 1.03<br>Oxidation:<br>n = 0.2 – 1.0<br>d = 0.46 – 0.84 |

| | | | |
|---|---|---|---|
| Tan et al. (2017) [32] | ▪ OC: ilmenite ore<br>▪ Fuel: Methane<br>▪ Total Pressure: 9 and 16 bar<br>▪ Temperature: 850 - 930°C | Phase-boundary controlled model with contracting sphere:<br>$kt = 1 - (1 - X_r)^{1/3}$ | P = 9 bar:<br>A = 0.17 $s^{-1}$<br>E = 28.2 kJ.$mol^{-1}$<br>P = 16 bar<br>A = 21.82 $s^{-1}$<br>E = 76.4 kJ.$mol^{-1}$ |
| Tan et al. (2017) [31] | ▪ OC: ilmenite ore<br>▪ Fuel: Methane, Natural gas mixture<br>▪ Total Pressure: 9 bar<br>▪ Temperature: 750 - 900°C | Phase-boundary controlled model with contracting sphere:<br>$kt = 1 - (1 - X_r)^{1/3}$ | E = 69 kJ.$mol^{-1}$ (pure $CH_4$)<br>E = 56 kJ.$mol^{-1}$ (Natural gas mixture) |
| Zhang et al. (2018) [50] | ▪ OC: $Fe_2O_3/Al_2O_3$<br>▪ Fuel: CO<br>▪ Total Pressure: 1 - 5 bar<br>▪ Temperature: 450 – 700°C<br>▪ Kinetic parameters obtained at atmospheric pressure | Adapted random pore model:<br>$k' = \frac{k'_{s,0} c_{CO,s} S_0 (1 - X)\sqrt{1 - \psi \ln(1 - X)}}{(1 - \varepsilon_0)(M_{Fe_2O_3} c_{CO,b})}$ | E = 102 kJ.$mol^{-1}$<br>$k_0$ = 1.8 x $10^{-3}$ (mol $m^{-2}$ $Pa^{-n}$ $s^{-1}$) |

## 3. Reactor analysis

In this section, the different reactor configurations proposed and investigated for pressurized chemical looping system are presented and discussed. The section is divided into four sub-sections: 1) Fluidized-bed, 2) Fixed-bed, 3) Moving-bed and 4) Rotating-bed reactors.

### 3.1. Fluidized-bed Reactor

The fluidized-bed reactor is the most widely used configuration for chemical looping systems [16]. For atmospheric operation, extensive investigations had been conducted using the dual circulating fluidized-bed reactor at a lab and pilot scales [16,52], however, fewer studies were reported for pressurized operation. In principle, the main effects of pressure on the fluidization characteristics are related to the increase of the gas density. Solid-solid interactions are not directly changed with elevated pressure due to the rigidity of the solids [53], but a denser gas increases the gas-particle drag, which also leads to less solid-solid collisions. As a result, it produces a more homogeneous gas-solid flow structure and decreases the incipient fluidization velocity.

Using electrical capacitance tomography (ECT), Rhodes et al. [54] revealed that for Geldart B particles, $U_{mf}$ slightly decreases with pressure whilst bed-voidage at $U_{mf}$ ($\varepsilon_{mf}$) was unaffected. Recently, the use of a borescopic technique was adopted to study the hydrodynamics of a fluidized-bed at elevated pressure [55]. The technique allows image visualization of the interior of the fluidized bed during the pressurized fluidization. The results revealed that, with increasing the pressure, the solids radial distribution becomes more or less uniform depending on the superficial gas velocity. Moreover, it was shown that the bubble size decreased in the central regions and increased near the wall regions with increasing the pressure [55]. Table 3 summarizes the effects of pressure on the main hydrodynamic parameters of fluidized-bed [56]. More extensive review on the effects of pressure on the hydrodynamic of fluidized-bed can be

found in Grace et al. [57] and Chaouki et al. [58]. The following sections presents the current research advancements on the use of fluidize-bed reactor for pressurized chemical looping applications.

**Table 3. Pressure effects on the hydrodynamics of fluidized-bed reactor.**

| Hydrodynamic parameter | Effect of pressure |
|---|---|
| Minimum fluidization velocity $u_{mf}$ | • Increasing pressure decreases $u_{mf}$. This effect becomes more pronounced as the particle size increases. |
| Bed voidage | • There is no clear correlation between pressure increase and bed expansion.<br>• $\varepsilon_{mf}$ is independent of pressure.<br>• $\varepsilon_{mb}$ increases with pressure for particles close to the group A-B boundary. |
| Bubbling characteristics | • High pressure results in smaller, more frequent bubbles. These effects are more pronounced for group A particles than for group B ones. |
| Entrainment and elutriation | • The bubble flow u-$u_{mf}$ increases with pressure, leading to higher entrainment rate.<br>• The terminal velocity decreases with increasing pressure (due to the increase in gas density), hence enhancing the entrainment/elutriation rate. |
| Hydrodynamic scaling | • Unlike atmospheric fluidized-bed reactors, cold flow laboratory model (operating with air at ambient temperature and atmospheric pressure) of a pressurized fluidized-bed at 12 bar and 860°C is approximately the same size as the commercial unit [59]. |

### 3.1.1. Dual circulating fluidized-bed reactor

Wang et al. [60] from Xi'an Jiaotong University conducted chemical looping combustion of coke-oven gas (COG) using a high-pressure circulating fluidized-bed system. Four types of oxygen carriers, composed of $Fe_2O_3$/CuO and $MgAl_2O_4$, have been investigated. The laboratory unit was designed for gaseous fuel for a fuel power range of 3-10 $kW_{th}$. The experiments were completed at a reactor pressure of 3 bar and temperatures up to 950°C. The experimental results showed that the COG conversion increases from 69.8% at 750°C to 92.33% at 900°C. After successful continuous operation of the unit for 15 hours, it revealed

high fuel reactivity, and all the OC maintained its stability. However, the 3 bar operation pressure could be too low to show the main challenges that may arise from a pressurized CLC system.

Xiao et al. [61] from Southeast University, China, carried out an experimental study on a 50 $kW_{th}$ pressurized dual circulating fluidized-bed reactor (Fig. 7) to investigate CLC of bituminous coal using an iron-based oxygen carrier. The FR and AR were designed to operate at fast fluidization and turbulent fluidization regimes, respectively. Three operating pressures have been studied (1, 3 and 5 bar) while maintaining temperature constant; 950°C in FR and 970°C in AR. High pressure operation was found to improve carbon conversion, $CO_2$ capture purity and combustion efficiency. This improvement was attributed to the combined positive effect that elevated pressure has on the iron oxygen carrier reduction and coal gasification. Controlling the experiments at elevated pressure encountered some difficulties compared to the atmospheric pressure operation. Solids elutriation rate increased with pressure due to a decrease in the FR cyclone capture efficiency at elevated pressure [61]. This challenge can be circumvented by dedicated cyclone design for a given elevated operating pressure.

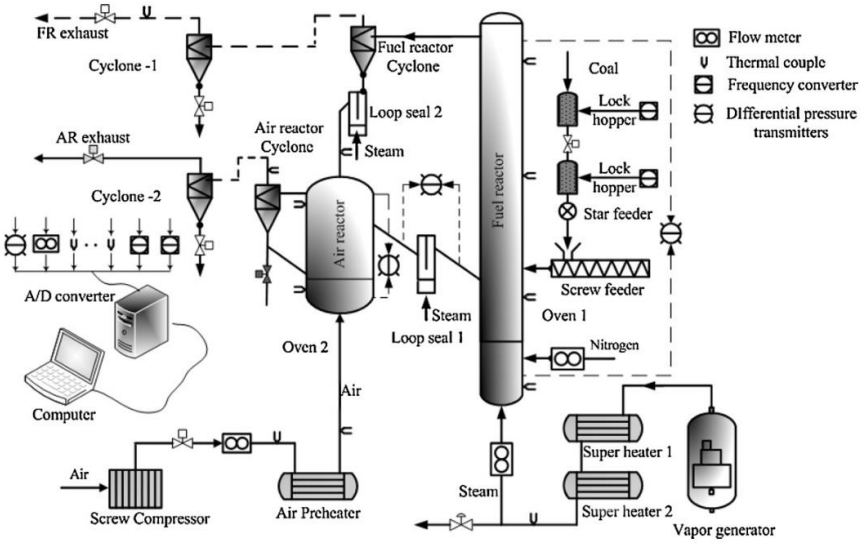


Fig. 7. A schematic diagram of the 50 $kW_{th}$ pressurized dual circulating fluidized-bed reactor [61], "Adapted with permission, Copyright (2012) Elsevier BV".

Another 50 $kW_{th}$ direct coal-fueled pressurized CLC unit is under development at University of Kentucky, USA [62]. They plan to use an iron-based OC developed from solid waste to provide catalytic gasification and improve coal combustion rate. More recently, a 0.5 $MW_{th}$ pressurized chemical looping system (Fig. 8) is under development at Korea Institute of Energy Research [63]. Conceptual design of the proposed unit by means of mass and energy balance calculations confirmed its feasibility. After successful installation of the unit, a hydrodynamic investigation was carried out that revealed a stable solid circulation at ambient temperature and atmospheric pressure for up to 7.5 hr. They plan demonstrating the unit with syngas delivered from a stand-alone coal gasifier unit operating at pressures up to 5.0 bar [63]. Another 0.6 $MW_{th}$ pressurized chemical looping combustion pilot-plant also under development at CanmetENERGY research center [64].

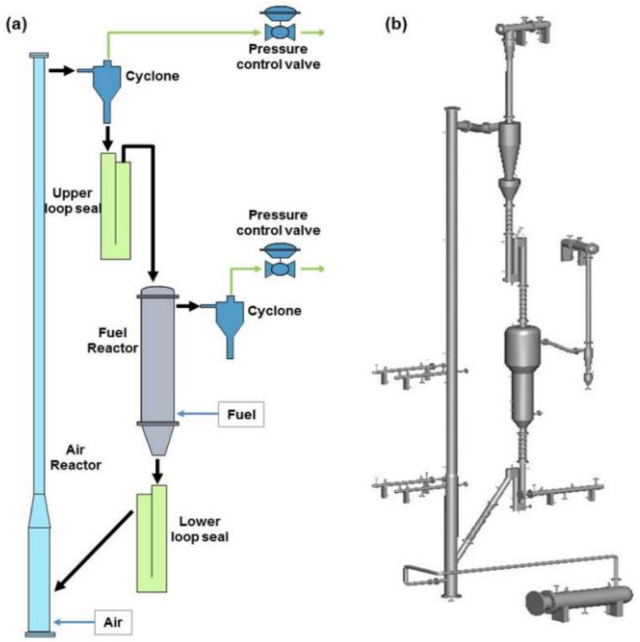


Fig. 8. A pressurized 0.5 MWth chemical looping combustion system, (a) schematic diagram, (b) 3D view [63].

### 3.1.2. Single fluidized-bed reactor

Several studies investigated the pressurized chemical looping process in a single fluidized-bed reactor to gain understanding of the pressure effect on hydrodynamics, fuel reactivity, product

selectivity and oxygen carrier integrity. Other researchers aimed to examine the potential of using a single fluidized-bed reactor as an alternative technology to the conventional dual-circulating fluidized-bed system; proposing the so-called gas-switching concept in which gases are alternated into a single fluidized-bed reactor. More details about the studies on this reactor configuration are given in the following section.

Ortiz et al. [7] from Instituto de Carboquı´mica (CSIC) utilized a semi-continuous fluidized-bed reactor to investigate the effect of the total pressure on chemical looping methane reforming to syngas. The effect of pressure was studied in the range of 1-10 bar using a Ni-based oxygen carrier and methane as fuel. The results of Ortiz et al. [7] showed that pressurized operation had no negative effect on the product distribution of the process. Methane conversion was above 98% at all operating pressures studied and no carbon formation was detected. Oxygen carrier characterization analyses before and after the pressurized experiments revealed no negative effect of the pressure [7].

Zhang et al. [25] from Southeast University studied a coal-fueled CLC in a single fluidized-bed reactor. The experiments were performed using iron ore as oxygen carrier while the operating pressures ranged between 1.0 and 6.0 bar at a constant operating temperature of 970°C. Carbon conversion increased with the pressure up to 5 bar, while further increase to 6 bar led to lower carbon and OC conversion (Fig. 9. ). Zhang et al. [34] proposed three phenomena that might explain the decrease of coal-fueled CLC performance at pressures higher than 5.0 bar:

1. Experimental results revealed higher $CH_4$ concentration at 6.0 bar, suggesting a shift in the thermodynamic equilibrium favoring methanation reaction of the mixture $H_2$, CO and steam (from the feed), thus decreasing the extent of oxygen carrier reduction.
2. Higher pressure suppresses the initial pyrolysis of coal gasification, decreasing the total volatile which leads to the decrease of char reactivity.

3. The inhibition effect of CO and $H_2$ on the coal gasification products could be more pronounced at high pressure.

The same unit of Zhang et al. [25] had been used in a fixed-bed mode running the pressurized coal-fueled CLC process at similar operating pressure and temperature conditions for comparison with the fluidized-bed mode. Similar trend of performance was observed in both modes, although the fixed-bed mode enhanced the carbon conversion compared to the fluidized-bed mode (Fig. 9. ). The lower carbon conversion in the fluidized-bed mode could be due to significant gas channeling led to poor mass transfer between the bubble and the emulsion phases, thus lowering the conversion of the gasification and volatiles products. On the contrary, the fixed-bed mode enhanced the gas-solid contact resulting in higher carbon conversion. However, sintering and agglomeration could happen due to excessive reduction of the iron-based oxygen carrier to iron or hot spot formation due to the highly exothermic oxidation reaction. When considering long-term stable coal-fueled CLC operation, the fluidized-bed mode is more favorable.

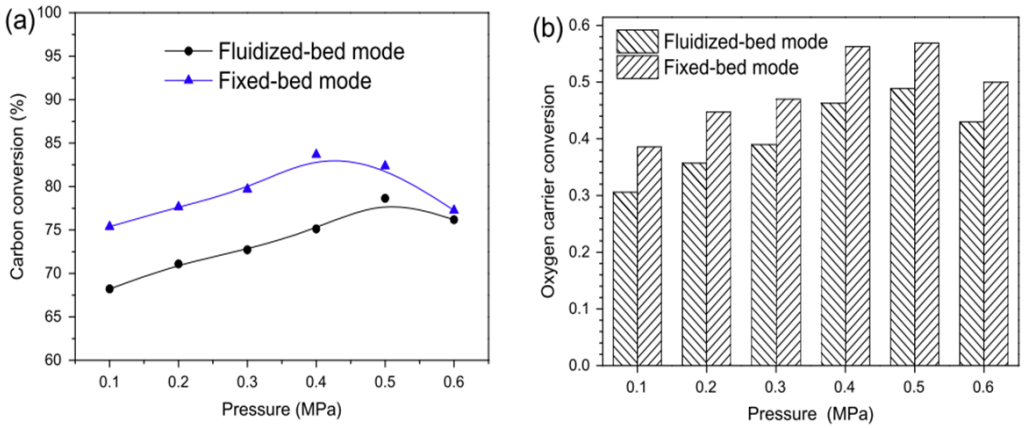


Fig. 9. Effect of pressure on carbon conversion and oxygen carrier conversion under fluidized-bed and fixed-bed conditions [25], "Adapted with permission, Copyright (2014) Elsevier BV".

Recently the gas switching concept has been proposed by SINTEF, Norwegian University of Science and Technology, and Eindhoven University of Technology [65–67]. In this configuration (Fig. 10), a cluster of reactors was employed to establish a continuous supply of

gases to downstream process components. Following are the main advantages of this concept compared to the dual circulating fluidized-bed reactor for chemical looping applications: 1) Solid circulation is intrinsically avoided, hence no need for complicated cyclone and loop seal for gas-solids separation. 2) Compact reactor design. 3) Better oxygen carrier utilization. 4) Reduced attrition rate of the OC particles due to gentler fluidization. 5) Simpler scale-up of chemical looping process due to the simple standalone nature of bubbling fluidized bed gas switching reactors.

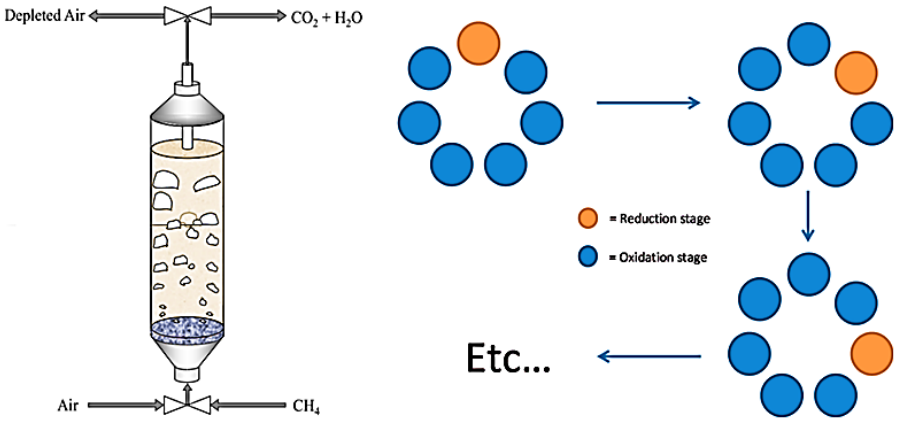


Fig. 10. A simplistic illustration of the gas switching reactor and the reactors cluster operating under the combustion mode; each disc represents one reactor [67,68], "Adapted with permission, Copyright (2013) ACS". This is an illustration reflecting that the oxidation step is six times longer than the reduction step requiring six reactors in the oxidation (large part of the feed air is used for removing the generated heat in the cycle with only a small part is used for reoxidizing the oxygen carrier) and only one in the reduction.

The dynamic operation of this concept can be challenging in a full-scale plant, because it would need a system of high temperature valves to be placed on the outlet of each reactor to switch between the stages (for most of the targeted processes where the downstream systems to integrated with the gas switching require high temperature gases). An additional challenge that arises from the transient nature of this process is the change in the temperature across the stage which may decrease the power plant electric efficiency. Nonetheless, with proper heat management strategies in the cycle [69], a coordinated cluster of gas-switching reactors can produce a continuous exhaust of pressurized hot stream suitable for a full-scale plant.

Experimental demonstration of the gas switching concept was achieved using a lab-scale reactor for CLC and CLR up to 5 bar pressure, using iron-based [70,71], ilmenite [65], Ni-based [67] and $CaMnO_{3-\delta}$ based oxygen carriers [66]. Gas switching combustion (GSC) using ilmenite showed that the pressure slightly improves the overall CO conversion confirming the results reported from TGA experiments with ilmenite when the superficial gas velocity was maintained constant [28]. This was attributed to the enhancement of diffusion resistance due to the change in the particle morphology. Using $CaMnO_{3-\delta}$ based oxygen carriers, negative effects of the pressure was found for CO conversion as in Zaabout et al. [66]. In this oxygen carrier, gaseous oxygen is released (through the well-known CLOU effect) and reacted with the fuel. This oxygen release is negatively affected by the pressure, thus leading to an overall decrease of fuel conversion rate as the pressure is increased. Note that, in these experiments, the molar gas flow rate was increased proportionally to the pressure in all the process stages to maintain a constant superficial velocity in the reactor thus cancelling out the negative effect of increased external mass transfer caused by the pressure as reported in TGA studies in Section 2. Using $H_2$ as fuel, revealed no effect of pressure on the reactor performance. Zaabout et al. [66] also conducted a parametric study to evaluate the effects of various parameters on the GSC reactor performance. Future development of the gas-switching concept will involve the use of a larger scale cluster of reactors to achieve continuous pressurized operation for various chemical looping technologies: combustion, reforming and water splitting [72].

Another concept employing the gas switching concept was proposed using a $H_2$-selective membrane for the production of pure hydrogen employing the concept of Chemical Looping Reforming [73]. In this concept, a single fluidized-bed reactor is used alternating oxidation, reduction and reforming reaction stages (Fig. 11). A $H_2$-selective membrane was inserted inside the fluidized-bed reactor for hydrogen recovery in the reforming stage. The main advantage of

hydrogen recovery is the shift of the reaction equilibrium towards larger methane conversion rates at lower operating temperature compared to SMR.

Experimental demonstration of the Membrane-Assisted Gas Switching Reforming concept (MA-GSR) was demonstrated at Eindhoven University of Technology (jointly with SINTEF and Norwegian University of Science and Technology) using a fluidized-bed reactor containing a Palladium-based membrane and a Ni-based oxygen carrier at operating pressures up to 5 bar as in Wassie et al. [73]. The reactor performance was studied at low temperatures (<550°C). The results illustrated pure hydrogen production with higher methane conversion (>50%) than the equilibrium level of the conventional fluidized-bed due to the use of membrane. The main limitation of the MA-GSR concept is the membrane stability, where defects were found on the membrane surface due to the harsh conditions of cyclic oxidation and reduction [73].

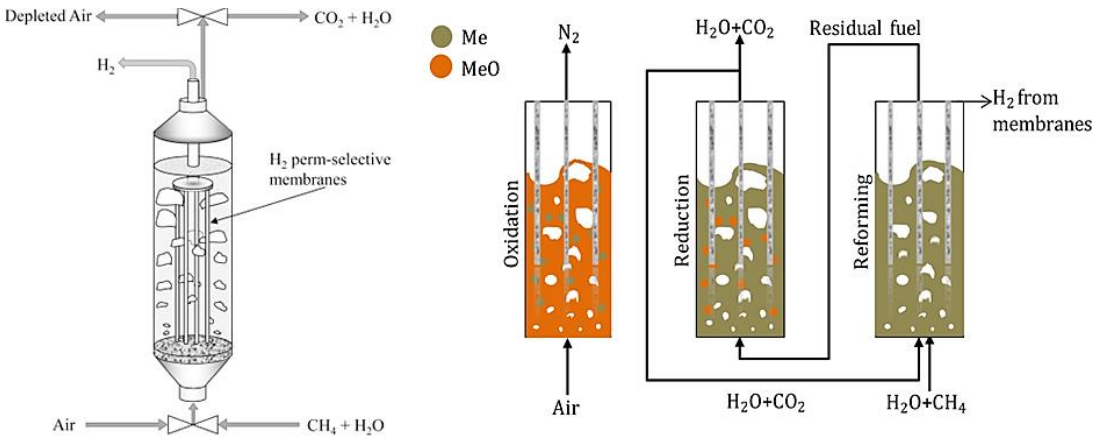


Fig. 11. Illustration of the membrane-assisted gas switching reforming reactor concept [74], "Adapted with permission, Copyright (2018) Elsevier BV".

### 3.1.3. Internally circulating fluidized-bed reactor (ICR)

The circulating fluidized-bed configuration remains an attractive option for chemical looping applications considering its steady-state nature and high achievable fluidization velocities. The needs for pressurized operation of chemical looping system inspired the development of a novel reactor configuration; the internally circulating reactor (ICR), which is based on the circulating fluidized-bed configuration but with simplified solids circulation mechanism to simplify

pressurized operation [75]. The ICR uses a single unit composed of two chambers connected with two simple ports (replacing the complex sealing system of the conventional CFB) and a freeboard (replacing the cyclone of the conventional CFB) (Fig. 12) [75,76]. In this way, the ICR simplifies the design, eases the solids circulation, and enables operating at high pressure easily in a single pressurized vessel. The oxygen carrier circulation in the ICR is attained through a higher gas velocity in the air reactor (AR) than in the fuel reactor (FR). This simple solids-circulation-mechanism combined with the compact design make the ICR concept very suitable for pressurized operation. The major trade-off of the simplicity obtained by the ICR concept is the gas leakage between the two reactor sections through the connecting ports, decreasing $CO_2$ capture efficiency and purity. However, the demonstration of the ICR concept by Osman et al. [77] (Fig. 12) for atmospheric CLC operation showed that the gas leakage can be minimized by controlling the fluidization velocity ratio of the two chambers and the solids inventory, achieving $CO_2$ capture efficiency and purity greater than 95%.

The ICR unit of Osman et al. [77] has also been used for chemical looping reforming of methane at atmospheric operation as in Osman et al. [76]. The reactor showed promising performance in term of gas leakage (up to 95% syngas purity), solids circulation rate, fuel conversion (up to 98% methane conversion) and revealed a simple approach to control its performance over a wide range of operating conditions.

An early study on ICR concept was developed by Chong et al. [78] for oil shale retorting, in which the shale and ash continually circulate between the two sections, while keeping the combustion gas and the retort product gases separate. The ICR concept has been further investigated by He et al. [79] and Fang et al. [80] for coal combustion and gasification processes. Further studies of ICR on chemical looping process were conducted at Chalmers University of Technology, where extensive experimental campaigns were carried out at atmospheric pressure [5,81–83]. The simplicity of the unit helped in providing a profound

knowledge about CLC and CLR performance for different oxygen carrier materials. Herguido et al. [84] also applied ICR concept for hydrogen separation using the steam-iron process at atmospheric pressure.

Recently, Osman et al. [85] successfully demonstrated the ICR unit for high-pressure chemical looping combustion using NiO-based oxygen carrier. The results showed a stable operation with high fuel conversion for about 40 hours of CLC operation at pressures up to 6 bar, achieving high $CO_2$ purity and capture efficiency up to 97%. The results of Osman et al. [85] also revealed that the solids circulation rate increases with increasing the operating pressure at constant superficial gas velocity.

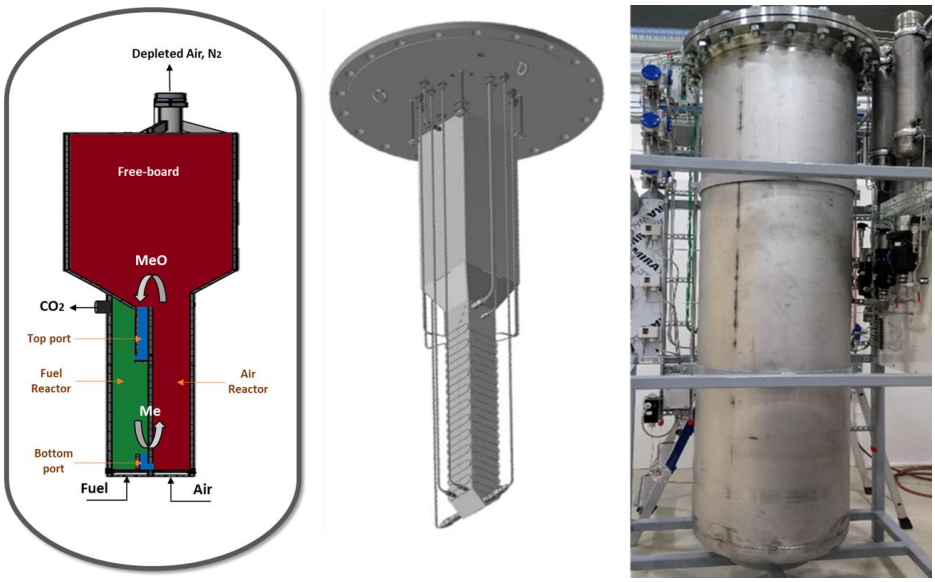


Fig. 12. A simplified scheme of the ICR design, CAD drawing of the ICR unit, and the ICR unit under operation inside the shell [76].

## 3.2. Fixed-bed Reactor

In the fixed-bed reactor system, the gas feeds are alternated to a fixed-bed of oxygen carrier to establish cyclic reduction and oxidation stages (Fig. 13), similar to the gas switching concept using fluidized-bed reactors discussed in section (3.1.2). The main benefits of this reactor concept are that solids circulation and solids attrition are intrinsically avoided, more compact reactor design with ease of pressurization in a single vessel [86]. The disadvantages of the

fixed-bed reactors are the requirement of a high temperature switching valve system (in most targeted processes), and highly exothermic oxidation reaction creates large transient thermal gradients that can damage the oxygen carrier by sintering or other defect on the morphological properties of the OC [87]. Additionally, larger particles should be used to minimize the pressure drop, which may lead to intra-particle diffusion limitation lowering the utilization of the oxygen carriers [88]. A direct comparison of packed and fluidized gas switching configurations concluded that the plug flow nature of packed beds makes this configuration most suitable for achieving high efficiencies and high $CO_2$ capture rates, but the material development is a large challenge due to the extreme thermochemical stresses imposed by the sharp heat and reaction fronts [89].

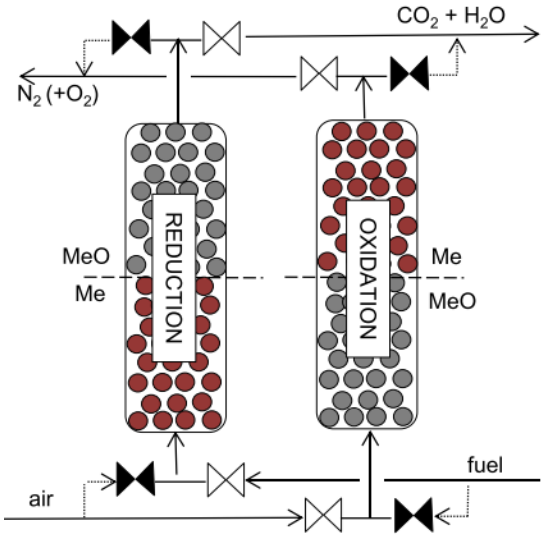


Fig. 13. A schematic diagram of a fixed-bed CLC reactor [90], "Adapted with permission, Copyright (2016) Elsevier BV".

Ishida et al. [91] used a fixed-bed reactor to study the effect of pressure on the reaction kinetics of chemical looping methane reforming to syngas with a Ni-based material as oxygen carrier. It was found that the reduction rate at moderately pressurized conditions (3 bar) was lower than atmospheric pressure reduction rate, attributing this to the endothermic reaction of methane

with NiO. Ishida et al. [101] suggested that increasing the $H_2O/CH_4$ ratio offer the capacity to improve the reactivity at high pressure.

Gallucci et al. [92,93] from Eindhoven University of Technology (TU/e) successfully demonstrated a cyclic steady state operation of chemical looping combustion of syngas in a 10 $kW_{th}$ pressurized fixed-bed reactor using NiO-based and ilmenite-based oxygen carriers. The reactor system has been demonstrated up to 7.5 bar. The mass flow rates were fixed during all experiments implying an increase in the residence time with the pressure. Using NiO-based oxygen carrier, the reactor performance at various pressure showed negligible effects of the pressure on the reduction and the oxidation cycle indicating that the increased gas residence time with the pressure had compensated the expected negative effects of gas dispersion and diffusion resistance to the particles. Carbon deposition enhanced at higher pressures, which could be the result of the higher level of oxygen carrier reduction achieved due to the higher fuel concentration as the pressure was increased. Addition of steam effectively suppressed carbon deposition, but also promoted CO conversion into $CO_2$ and $H_2$ through the WGS reaction. The maximum temperature rise achieved in the cyclic reduction/oxidation was 340°C with possibility of autothermal operation (no external heat supply) after about three full cycles.

Using a fixed-bed reactor, pressurized hydrogen production with chemical looping water splitting system was investigated by a research group at Graz University of Technology [94–98]. The authors proposed a new concept that combines conventional steam reforming and the steam-iron process in a single fixed-bed reactor containing both the oxygen carrier and the reforming catalyst (Fig. 14). The process involved the following steps: 1) catalytic hydrocarbon reforming to syngas, 2) reduction of the iron-based OC using syngas, and 3) oxidation of the reduced OC using steam to produce pure hydrogen. Based on thermodynamic analysis they revealed that the oxidation could be achieved at pressurized conditions, however, the reforming and the reduction step should be carried out at atmospheric pressure to maximize the

conversion efficiency [94]. The experiments of Zacharias et al. [98] were carried out at atmospheric pressure for the reforming/reduction step and at high pressure up to 95 bar for the steam oxidation step. The results revealed no negative effect of the elevated pressure on the reactor performance in the oxidation stage. High purity hydrogen was attained in the range of 99.95-99.999% with CO and $CO_2$ only as impurities given that no air feed is needed in the process. The practicality of operating the oxidation and reduction stages at very different pressures and the feasibility of autothermal operation of the process are potential challenges of this configuration.

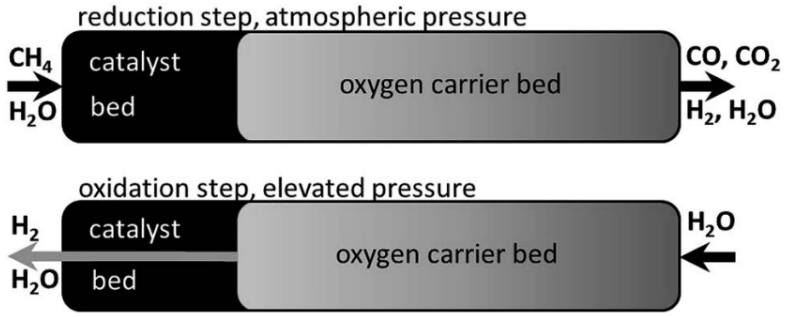


Fig. 14. The reformer steam-iron process schematic in a fixed bed reactor [96], "Adapted with permission, Copyright (2016) RSC".

In-situ solid-fuel gasification under CLC mode has been investigated in a high-pressure fixed-bed system at Southeast University [99–101]. The study focused on the pressure effects on the cyclic performance rather than the reactor design, operation and scale-up. Chinese bituminous coal was used as fuel together with different types of iron ore-based oxygen carriers, while steam was used as a gasification agent. Initial investigation by Xiao et al. [99] for up to 5 reduction/oxidation cycles showed that the reduction rate increased with pressure up to 5 bar then slightly decreased at 6 bar. Subsequent study of 20 reduction/oxidation cycles showed an improvement of the reaction rate with increasing the pressure, which was attributed to the increase of the steam partial pressure and the gas residence time, thus simultaneously enhancing the coal char gasification and reduction of the iron ore [100,101].

The utilization of bulk monolithic OC for CLC in a fixed-bed reactor has been proposed by Gu et al. [102] to limit the temperature fluctuations, minimize the pressure drop and to decrease the intra-particle diffusion limitation associated with the use of large pellets in fixed-beds system. The results of Gu et al. [102] showed high activity of Ce-Zr-F-O/$Al_2O_3$ oxygen carrier for methane combustion as a result of the strong active component to support interaction, that was similar to that of the powder oxygen carrier. Zhang et al. [103,104] extended this concept to a 10 $kW_{th}$ prototype using a honeycomb CLC reactor (Fig. 15) with NiO-based and iron-based oxygen carriers. The results of Zhang et al. [103,104] showed superior performance in term of methane conversion, reduction kinetic, overall reactor stability and limited cyclic temperature fluctuation (50 K) benefiting from the homogeneous distribution of the reaction heat inside the surface of the honeycomb reactor. These preliminary studies proved the feasibility of the concept, but pressurized CLC operation using the monolithic structure yet to be completed to demonstrate the full potential of this configuration in solving the technical challenges facing pressurized chemical looping systems.

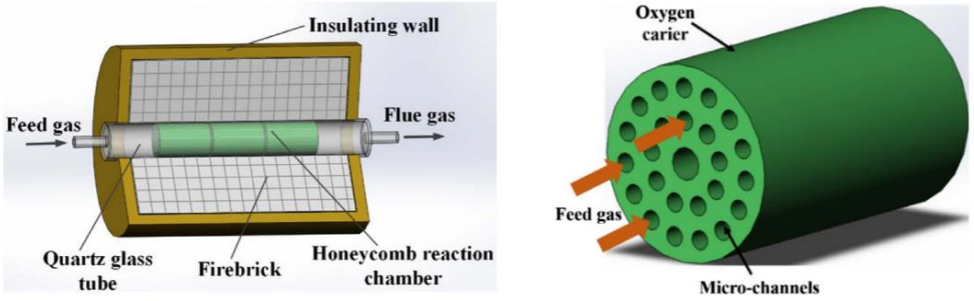


(a) Configuration of the central section (b) Honeycomb chamber

Fig. 15. Illustration of the honeycomb CLC reactor [104], "Adapted with permission, Copyright (2018) Elsevier BV".

## 3.3. Moving-bed Reactor

The moving-bed reactor designed with gas-solid countercurrent contact pattern can achieve higher fuel conversion and higher oxygen carrier utilization compared to the conventional CFB,

thus presenting new prospects in chemical looping applications. In addition, moving-bed reactors offer minimal particles attrition, and encounters low pressure imbalances across dual reactors as the operating gas velocity is below the minimum fluidization velocity of the OC particles and hence would be easier to operate under high pressure compared to fluidized-bed reactors. However, the low gas velocity to keep the particles falling against the gas flow requires large reactor vessels that would result in a larger footprint compared to the conventional circulating fluidized bed configuration. This drawback could however be minimized by using large oxygen carrier particles, but this brings challenges associated with mass and heat transfer limitations within the oxygen carriers imposing the use of engineered oxygen carrier with high production costs.

A research group at Ohio State University carried out extensive studies on the potentiality of applying the moving-bed reactor concept in chemical looping for hydrogen production with inherent $CO_2$ separation, using the steam iron-process [105–108]. The research group developed a process named syngas chemical looping (SCL), utilizing an iron-based OC and consists of three reactors namely the reducer, the oxidizer, and the combustor (Fig. 16). In the reducer, a coal-derived syngas was used to reduce $Fe_2O_3$-based OC to a mixture of Fe and FeO, while producing a mixture of $CO_2$ and steam. In the oxidizer, pure hydrogen produced by using the steam-iron process in which steam is used to partially oxidize the reduced OC into $Fe_3O_4$. In the combustor, the oxidized $Fe_3O_4$ particles are further oxidized to $Fe_2O_3$ to allow a complete cycle while providing the necessary heat to the process through the exothermic oxidation reaction. The reducer and the oxidizer are operated in a moving-bed mode to counteract the equilibrium limitation of the involved reactions thus maximizing fuel, oxygen carrier and steam conversion. The combustor operates as a fluidized-bed mode to fully oxidize the OC and to transfer the solids back to the reducer. Thermodynamic analysis carried out by Li et al. [107] showed that higher fuel and oxygen carrier conversions can be obtained in moving-beds than

in fluidized-beds. This will decrease the required solid circulation rate, minimizing the reactor volume, and maximizing the overall efficiency of the process.

The demonstration of the SCL process has successfully been validated using a 2.5 $kW_{th}$ bench scale unit and a 25 $kW_{th}$ sub-pilot scale unit [105–108]. The concept of the counter-current moving-bed reactor confirmed that nearly pure $H_2$ could be produced with full syngas conversion to $CO_2$ and $H_2O$. Following these outcomes, a 250 $kW_{th}$ pressurized syngas chemical looping pilot plant has been commissioned and successfully demonstrated the concept as in Hsieh et al. [109]. The first operation of the SCL pilot plant was completed at 10 bar and resulted in syngas and OC conversion close to the thermodynamic limits validating the benefit of using the moving-bed configuration in the reducer and the oxidizer [109]. Yet, a techno-economic assessment taking in consideration the results from the pilot demonstration campaign is needed to confirm the potential of the moving bed in bringing down the cost of hydrogen production through this process.

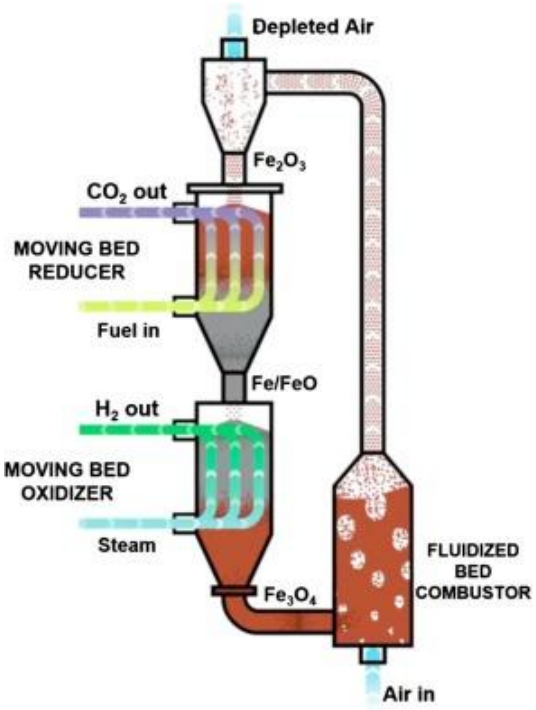


Fig. 16. A conceptual design of syngas chemical looping pilot unit with a counter-current moving bed reducer and oxidizer reactors [109], "Adapted with permission, Copyright (2018) Elsevier BV".

## 3.4. Rotary-bed Reactor

The rotary-bed reactor is an extended version of the fixed-bed reactor, in which the oxygen carrier particles are placed in a rotating fixed-bed while a static fuel and air flow radially outward through the rotating-bed [110,111]. Fig. 17 shows an illustration of a rotary-bed reactor divided to four sections for air, fuel and two inert gas sectors in-between to avoid gas leakage between the air and fuel zones. The main advantages of this concept are the separation of gas and solids is intrinsically avoided, the compactness of the reactor, continuous operation without the need of solids circulating and scale-up potential [111]. These advantages facilitate the operation at high pressure offering prospects for higher process efficiency, but challenges with gas leakage between air and fuel sections, temperature fluctuation and oxygen carrier thermal expansion should be expected [111]. A limited number of studies have investigated the feasibility of rotary-bed reactors applied to chemical looping restricted to atmospheric conditions. Blom et al. [110,112,113] conducted a series of experimental studies on a lab-scale rotary-bed reactor using CuO-based oxygen carrier and methane, achieving 90% fuel conversion, 90% $CO_2$ capture efficiency and up to 65% $CO_2$ purity. Ghoniem et al. [111,114–119] focused on modelling and techno-economic assessment of chemical looping in this configuration. More research is still needed, especially experimental studies under high pressure, in order to comprehend the feasibility of the concept.

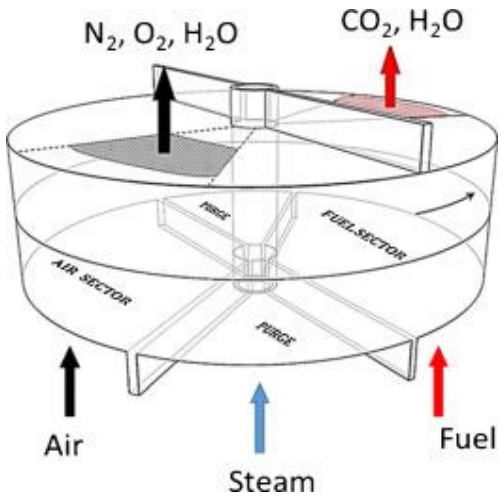

Fig. 17. Simple illustration of the rotary-bed reactor [117], "Adapted with permission, Copyright (2015) Elsevier BV"..

### 3.5. Summary of different pressurized reactor configurations

Table 4 provides a qualitative comparison of different pressurized chemical looping configurations over a range of important performance measures. A simple scoring system was used to highlighting the pros and cons of each configuration. The comparison shows that each configuration has strengths and weaknesses. Thus, the choice between these configurations will depend on the relative importance of the different performance criteria for a given application.

The dual CFB has received the highest research focus for chemical looping and reached the highest TRL level, but with very limited studies under pressurized conditions. This gives limited grounds for judging its suitability to pressurized operation. Nevertheless, the key uncertainty arises from the stability of solids circulation in a closed loop involving many components; two reactors operating at different fluidization regimes, cyclones and loop seals. The internally circulating reactor (ICR) configuration has the potential to retain most of the advantages of dual CFB configuration, but with scarifying a small losses in separation efficiency. Values above 90% $CO_2$ purity and capture efficiencies were achieved at operating pressures up to 6 bar, which is promising against the large design simplification brought by this configuration. Improved port design could further improve $CO_2$ separation performance [77]. Packed and fluidized bed switching based concepts has received the second largest focus with dozens of studies completed for different chemical looping processes. Pressurized operation proved to be simple for these configurations, but the high temperature valve to be placed on the outlet of each reactor in the cluster, remains the highest uncertainty. Solving this challenge could be compromised by operating the process at lower temperature or applying an additional firing step to boost the temperature of the gas stream before being sent to the downstream power train. However, this would result in reduced $CO_2$ capture efficiency if

natural gas is used for added firing and higher costs if hydrogen is used. The relative pros and cons of the fluidized and fixed bed configurations are related to their fundamental behavior as well mixed and plug flow reactors, respectively.

The moving-bed reactor is the most suitable for chemical looping processes involving thermodynamically limited reactions such as the steam-iron process. The large reactor footprint imposed by the need to operate at gas superficial velocities below minimum fluidization could be reduced by using large particles, but this measure will be compromised by the increased mass and heat transfer resistance in the particle. The rotating bed is the least developed, and high-pressure operation is yet to be demonstrated.

Table 4: Comparison of different reactor configurations for pressurized chemical looping: Advantage (+), Neutral (o), Disadvantage (-).

| Reactor configuration | Experience with pressurized operation | Ease of scale-up | Ease and flexibility of operation | Small plant footprint | Mechanical stresses on the OC | Thermo-chemical stresses on the OC | $CO_2$ separation efficiency | Others |
|---|---|---|---|---|---|---|---|---|
| **Dual CFB** | Limited | - | - | + | - | + | + | + (highest TRL, but under atmospheric conditions) |
| **Gas switching** | Fair | + | + | - | o | + | o | - (need for high temperature valves) |
| **ICR** | Limited | o | o | o | o | + | o | o (Connecting ports design requires further optimization) |
| **Packed bed** | Fair | + | o | - | + | - | + | - (need for high temperature valves) |
| **Moving bed** | Limited (restricted to the steam-iron process) | o | - | - | o | o | + | + (high conversion for equilibrium reactions) |
| **Rotating bed** | None | + | o | o | + | - | - | Not enough experimental demonstration to judge it |

Table 5 gives an overview of the current development of the different reactor configurations. Clearly, most configurations are demonstrated at pressures well below the targeted operating pressure for the respective industrial applications (20-40 bar). In addition, no configuration has

thus far reached the MW-scale required for proper identification of scale-up challenges. Further R&D investments are needed to demonstrate successful operation under industrially relevant pressures at pilot scale. Such demonstration studies will facilitate a better understanding of the relative importance of the qualitative performance criteria discussed in Table 4, allowing further scale-up efforts to focus on the most promising configurations.

Table 5: Current level of development of different reactor configurations for pressurized chemical looping.

| | **First proposed (year)** | **Largest scale (kW)** | **Highest pressure (bar)** | **Pressurized CL technologies demonstrated** |
|---|---|---|---|---|
| **Dual CFB** | 2001 | 50 | 5 (50 kW) | Solid fuel CLC |
| **Gas switching** | 2013 | 60 | 5 (2 kW) | Combustion and reforming |
| **ICR** | 2016 | 4 | 6 (3 kW) | Combustion |
| **Packed bed** | 2007 | 100 | 100 (10 kW) | Combustion, reforming, steam-iron process |
| **Moving bed** | 2010 | 250 | 10 (250 kW) | Steam-iron process |
| **Rotating bed** | 2011 | 0.5 | 1 (0.5 kW) | Combustion |

## 4. Techno-economic Analysis

Pressurization of the chemical looping systems is of interest for increasing the overall process efficiency. In power production, for example, a pressurized combustion process can utilize a combined power cycle instead of only a Rankine cycle. The former can achieve efficiencies of 64% (modern natural gas combined cycle plants), whereas the latter achieves about 45% efficiency (modern supercritical pulverized coal power plants). In hydrogen production, high pressure reforming is essential to facilitate hydrogen production in a pressure swing adsorption (PSA) unit without having to invest a large amount of compression work. Many other chemical

processes consuming syngas also operate at high pressures, implying that large compression work savings are possible if the reforming process also takes place at high pressures.

Even though pressurized equipment is more expensive for a given size, equipment size reduces under pressurized conditions to limit any increases in CAPEX. Furthermore, due to higher pressure the energy required for $CO_2$ compression will be reduced significantly. Due to these advantages of pressurized operations, the production cost will be cheaper than that of non-pressurized systems for most gas-fueled processes. Consequently, several technical and economic studies of chemical looping concepts either for power production or hydrogen generation or with diverse plant integrations have been conducted for pressurized conditions. These studies show the promise of this concept at large scale. The results from several recent studies are summarized in Table 6 and Table 7. Even though levelized costs of electricity (LCOE) and hydrogen (LCOH) from the various studies varied widely due to different economic assumption employed, most studies reported that pressurized chemical looping configurations significantly outperformed reference plants based on conventional $CO_2$ capture technologies. These studies are reviewed in more detail below.

**Table 6:** Summary of the techno-economic studies on power generation using pressurized chemical looping concepts (in 2019 $) (*without $CO_2$ capture)

| **Reference** | Technology | Pressure (bar) | Electrical efficiency (LHV) | LCOE ($/MWh) | $CO_2$ avoidance cost ($/ton) | Reference plant efficiency (LHV) | Reference plant LCOE ($/MWh) |
|---|---|---|---|---|---|---|---|
| Ogidiama et al. (2018) [120] | Chemical looping combustion with combined cycle plant | 15 | 55.6% | 55.4 | 26.3 | 50.6% | 58.3 |
| Zhu et al. (2018) [121] | Chemical looping combustion with combined cycle plant | 6-18 | 50.1% | 74.5 | - | 49.4% | 88.2 |
| Porrazzo et al. (2016) [122] | Chemical looping combustion with combined cycle plant | 10 | 52.0% | 85.1 | - | 51.0% | 120.0 |
| Ogidiama et al. (2018) [123] | Solar assisted chemical looping combustion with absorption chiller | 15 | 63.4% (thermal) | 46.8 | - | - | - |
| Diglio et al. (2018) [124] | Fixed bed chemical looping combustion with gas turbine cycle | 20 | 51.0% | 56.7 | 33.7 | 55.0%* | 46.0* |
| Iloeje et al. (2018) [125] | Rotary Chemical looping combustion with Brayton cycle plant | 5 | 56.0% | 52.5 | - | - | - |
| Khan et al. (2020) [126] | Chemical looping combustion with combined cycle plant | 22 | 50.7% | 97.0 | 117.3 | 54.0% | 91.2 |
| Khan et al. (2020) [126] | Chemical looping combustion with additional combustor fired by NG | 22 | 60.7% | 73.0 | 60.3 | 54.0% | 91.2 |
| Khan et al. (2020) [126] | Chemical looping combustion with additional combustor fired by $H_2$ | 22 | 60.7% | 91.0 | 96.3 | 54.0% | 91.2 |
| Mancuso et al. (2017) [127] | Chemical looping combustion with coal-fired and IGCC | 17 | 40.8% | 116.4 | 37.0 | 35.3% | 128.1 |
| Cloete et al. (2018) [128] | Chemical looping combustion and oxygen production IGCC | 17 | 45.4% | 85.6 | 50.1 | 37% | 104 |
| Farooqui et al. (2018) [129] | Chemical looping syngas production with oxy-fuel combined cycle plant | 2 | 50.7% | 122.3 | 96.3 | 54.9%* | - |
| Nazir et al. (2018) [130] | Chemical looping reforming with combined cycle power plant | 18 | 43.4% | 132.7 | 183.1 | 49.5% | - |
| Nazir et al. (2018) [131] | Gas switching reforming | 18 | 47.4% | 115.3 | 123 | 58.4%* | 84.1* |

**Table 7:** Summary of the techno-economic studies on hydrogen generation using pressurized chemical looping concepts (in 2019 $) (*without $CO_2$ capture)

| **Reference** | Technology | Pressure (bar) | Efficiency (LHV) | LCOH ($/kg) | $CO_2$ avoidance cost ($/ton) | Reference plant efficiency (LHV) | Reference plant LCOH ($/kg) |
|---|---|---|---|---|---|---|---|
| Nazir et al. (2020) [132] | Gas switching reforming | 33 | 80% | 1.8 | 18.0 | 79.3%* | 1.9* |
| Wassie et al. (2018) [133] | Membrane-assisted gas switching reforming | 50 | 81% | 3.5 | 89.5 | 67.0% | 3.6 |
| Spallina et al. (2016) [134] | Membrane-assisted chemical looping reforming | 50 | 82% | 2.3 | -40.7 | 67.0% | 3.6 |
| Spallina et al. (2017) [135] | Chemical looping reforming | 20 | 75% | 3.6 | 99.6 | 67.0% | 3.7 |
| Cloete et al. (2019) [136] | Membrane assisted autothermal reforming | 50 | 81% | 1.72 | - | 80.0% | 1.7 |
| Khan and Shamim (2016) [137] | Three reactor chemical looping reforming with combined cycle plant | 20 | 71.8% | 1.9 | - | - | 2.7 |
| Khan and Shamim (2019) [138] | Three reactor chemical looping reforming with combined cycle plant | 20 | 74.5% | 1.7 | - | - | 2.7 |
| Chisalita and Cormos (2019) | Chemical looping hydrogen production | 30 | 75.8% | 1.5 | 21.2 | 74.1% | 1.6 |
| Chisalita and Cormos (2019) [139] | Sorption enhanced chemical looping reforming | 30 | 70.4% | 1.8 | 65.6 | 74.1% | 1.6 |
| Xiang and Zhou (2018) [140] | Chemical looping hydrogen generation using coke oven gas | 10 | 68.5% (exergetic) | 2.9 | - | - | - |

## 4.1. Chemical looping combustion

A lot of attention has been given to the primary concept of chemical looping for power generation. Below are the summaries of several such recent studies focusing on techno-economic assessment of pressurized chemical looping combustion. Ogidiama et al. [120] conducted a detailed performance and economic comparison between the natural gas-fired CLC-based power plant with that of a conventional natural gas-fired combined cycle power plant with post-combustion $CO_2$ capture. A simple CLC cycle was employed with cycle pressure of 15 bar and NiO as the OC. The $CO_2$ capture costs shown in Table 6 are low compared to a review of CCS costs by Rubin et al [3], 48 - 111 $/ton.

Zhu et al. [121] presented the techno-economic performance of a CLC plant employing different OCs (Fig. 18). The net electrical efficiencies reported were in the range 45 to 50% due to difference in turbine inlet temperature (TIT). The corresponding levelized cost of electricity ranged from 75 to 89 $/MWh, in which nickel has the lowest LCOE (due to its ability to facilitate high temperature operation) followed by ilmenite and copper. It was reported that an increase in pressure (6-18 bar) initially decreased the cost of electricity (105.3 – 74.5 $/MWh). With a further increase in pressure, the cost of electricity increased indicating the requirement of an optimal pressure ratio that resulted in maximum power output at a specific TIT.

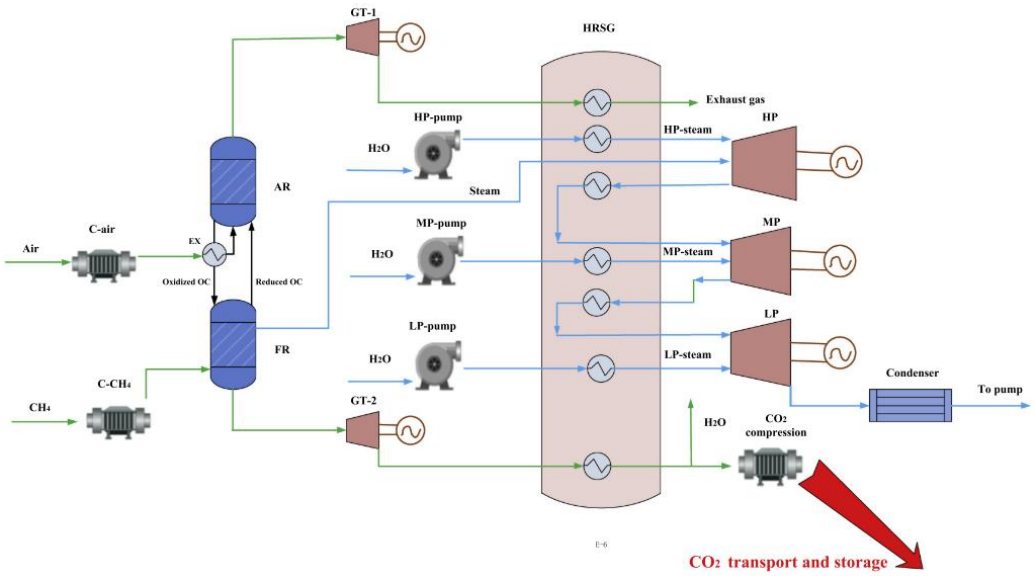


Fig. 18. Configuration of chemical looping combustion for power generation [121], "Adapted with permission, Copyright (2018) Elsevier BV".

Porrazzo et al. [122] developed a system level model of the CLC process integrated with a combined cycle power plant. Detailed fluidized bed models considering the kinetics and hydrodynamics were implemented for the CLC reactors in the plant model. Nickel-based OC was used and the cycle was operated at a pressure of 10 bar. The net electrical efficiency was 1%-point better than the reference plant with 20% less LCOE.

Ogidiama et al. [123] used the chemical looping concept to utilize waste heat effectively. A CLC cycle integrated with a combined cycle plant was compared with a CLC cycle integrated with an absorption chiller plant. In both configurations, the CLC plant was operated at a pressure of 15 bar. A parabolic trough solar system was used to direct solar energy onto the fuel reactor, acting as an additional heat source for the endothermic fuel reaction. The results showed that by integrating with an absorption chiller and waste heat utilization potential of 49%, the overall plant efficiency can be significantly increased.

Diglio et al. [124] proposed a fixed bed CLC reactor network for small-scale power generation (Fig. 19. ). The proposed configuration consisted of four fixed bed reactors in parallel operated

at 20 bar. A copper-based OC was used in the fixed beds which allowed an exothermic reaction in both the oxidation and reduction stages. The reactors were arranged in a way such that two separate gas streams were obtained continuously, similar to that in conventional CLC system. The air stream was expanded for power generation while the $CO_2$ stream was used to preheat the fuel.

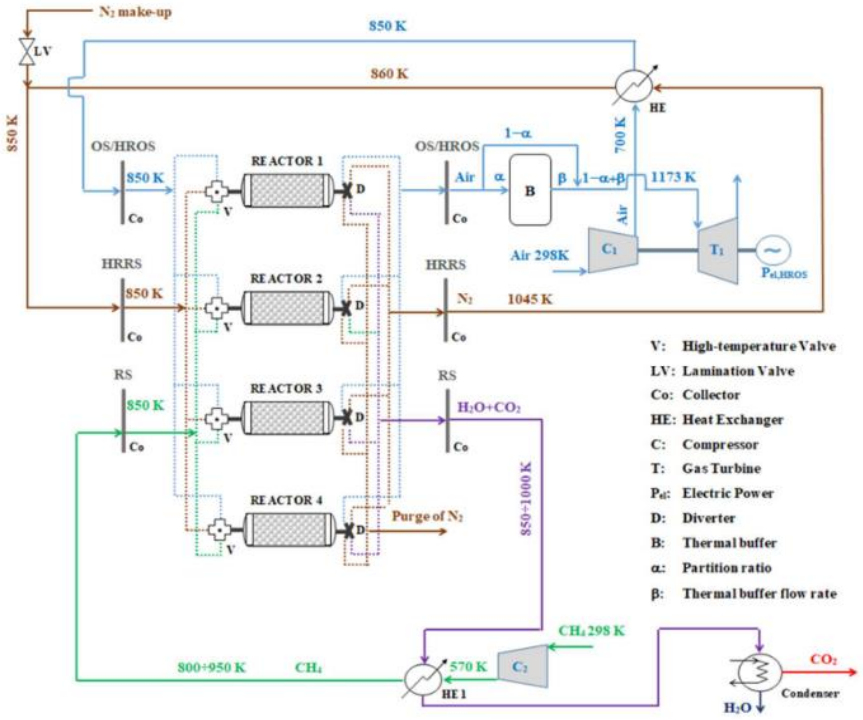


Fig. 19. Layout of the CLC process integrated with stationary power plant [124], "Adapted with permission, Copyright (2018) ACS".

Iloeje et al. [125] developed a rotary CLC reactor which comprises of the OC in the form of closely packed microchannels. The objective of this design was to minimize the losses in efficiency associated with heat transfer in the reactor. The base case reactor configuration was operated at 5 bar and was integrated with a recuperative Brayton cycle plant. By varying the pressure ratio from 3 to 7 bar, it was reported that the net thermal efficiencies were increased by more than 2%-points with significant reduction in LCOE.

The natural gas-fired CLC configurations reviewed thus far all suffer from a fundamental problem: the maximum achievable reactor temperature is far below the firing temperature of

modern gas turbines. Thus, although CLC imposes almost no direct energy penalty for $CO_2$ capture, the indirect energy penalty involved in running the combined power cycle from a lower starting temperature is considerable. Depending on the CLC reactor temperature selected and the reference plant TIT, the resulting power plant efficiency can be well below that of NGCC benchmarks with post-combustion $CO_2$ capture [142]. This problem can be mitigated by including an additional combustor downstream of the CLC reactors to increase the stream temperature to the operating level of the gas turbine. Khan et al. [126] recently conducted a techno-economic assessment of such a power plant configuration (Fig. 20), finding that added firing with natural gas results in significantly lower $CO_2$ avoidance costs than a benchmark NGCC plant with post-combustion $CO_2$ capture. However, $CO_2$ avoidance is only 52.4% due to emissions from the added firing. When hydrogen firing is used instead, the cost of hydrogen production is very important to power plant economics. The study also confirmed that a CLC plant without added firing is less attractive than conventional NGCC with post-combustion $CO_2$ capture.

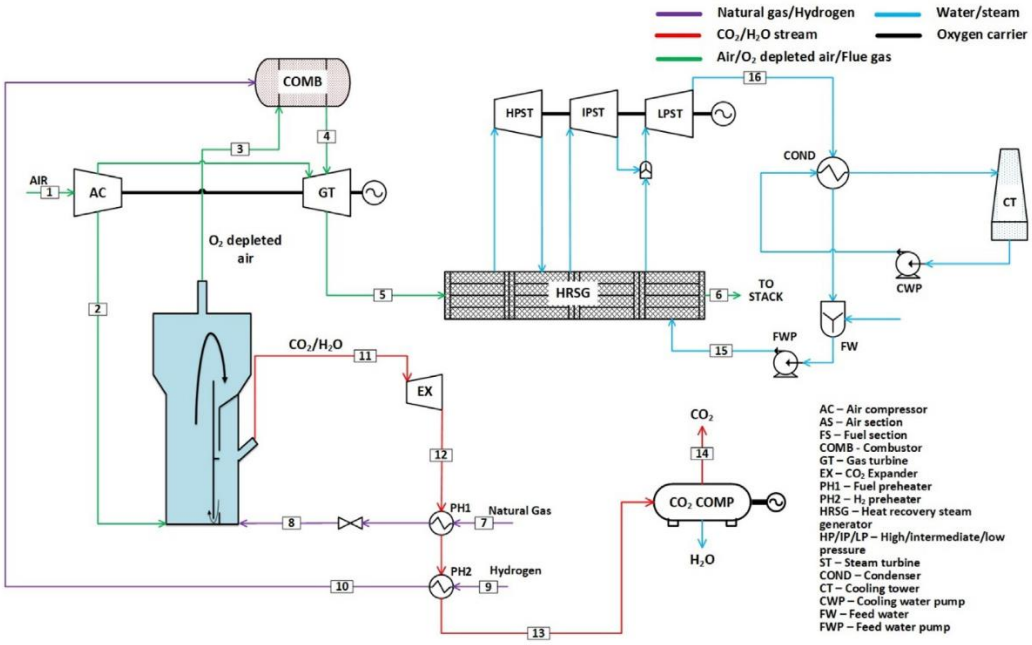


Fig. 20. Layout of the CLC process integrated with stationary power plant [126], "Adapted with permission, Copyright (2020) Elsevier BV ".

The attractiveness of chemical looping concepts can be further increased by integrating them with coal-fired plants or integrated gasification combined cycle plant. Mancuso et al. [127] conducted a comprehensive economic-assessment on integrated gasification combined cycle (IGCC) and supercritical-pulverized coal plants with different configurations. The IGCC plant with CLC was based on the packed bed reactor concept. The syngas produced from the gasification was fed to the reduction reactor of the packed bed CLC process. The CLC cycle was operated at a pressure of 17 bar with ilmenite as an OC. An increase in net electrical efficiency by 5%-points and a reduction in LCOE by 9% with respect to the reference plant (IGCC plant with conventional pre-combustion $CO_2$ capture) was reported.

The aforementioned packed-bed CLC plant was integrated with a chemical looping oxygen production (CLOP) unit to increase the efficiency by 2.3 %-points [12]. The use of hot gas clean-up technology offered a further 2 %-point efficiency gain for a final efficiency of 45.3%. Despite the good thermodynamic performance, a subsequent economic assessment [128] found limited improvements in cost from including the CLOP unit due to the increase in size of the gasifier and gas clean-up units resulting from the lower heating value of the syngas produced. However, the LCOE still compared favorably against other clean energy technologies (nuclear, wind and solar). The benefits of operating this plant with biomass for negative emissions in a scenario with high $CO_2$ prices was also illustrated.

As was the case with natural gas-fired combined cycles, substantial gains in efficiency can be achieved in a CLC-IGCC power plant by including an added combustor to raise the TIT to that of the benchmark plant. In addition, a recuperator recovering the heat form the reduction stage to pre-heat the air can provide further efficiency gains. When these improvements are combined with the ability of the CLC plant to recover some heat from steam condensation and the potential to remove pre-combustion gas treatment, a very high efficiency could be achieved

eliminating the $CO_2$ capture energy penalty [144]. In this case, natural gas was used in the added combustor to raise the temperature from 1165°C to 1370°C.

An important fundamental limitation of IGCC power plant configurations is the low flexibility of the gasification train, making such plants incompatible with future power systems containing large shares of fluctuating wind and solar power. In this respect, the OC can be exploited as an energy storage medium enabling variable power output from a constant stream of syngas input and $CO_2$ output. Such a plant requires complete uncoupling of the gasification train and the power cycle to allow for flexible operation and was recently proposed based on GSC reactors integrated with a HAT power cycle [145]. When a low-cost slurry-fed gasifier was employed, the plant could achieve 41.6% efficiency with high $CO_2$ capture.

## 4.2. Chemical looping reforming

Chemical looping reforming for syngas generation has also been extensively studied for pressurized operations. Generally, for hydrogen production, the syngas generated is subjected to water-gas shift reactors followed by pre-combustion $CO_2$ capture by conventional monoethanolamine systems. The hydrogen rich gas is then burned in a combined cycle power plant.

Farooqui et al. [129] compared the performance of an oxy-fuel combined cycle plant integrated with chemical looping syngas production (OXY-CC-CL) with a conventional NGCC and a natural gas-based oxyfuel combined cycle (OXY-CC) plants (Fig. 21). In the fuel reactor, $CO_2/H_2O$ dissociation was considered to produce syngas through partial oxidation of the reduced OC. The plant was operated at a lower pressure (2 bar) which increased the investment costs and the energy consumption for $CO_2$ compression to high pressures. Consequently, the LCOE reported was significantly higher than the conventional technologies.

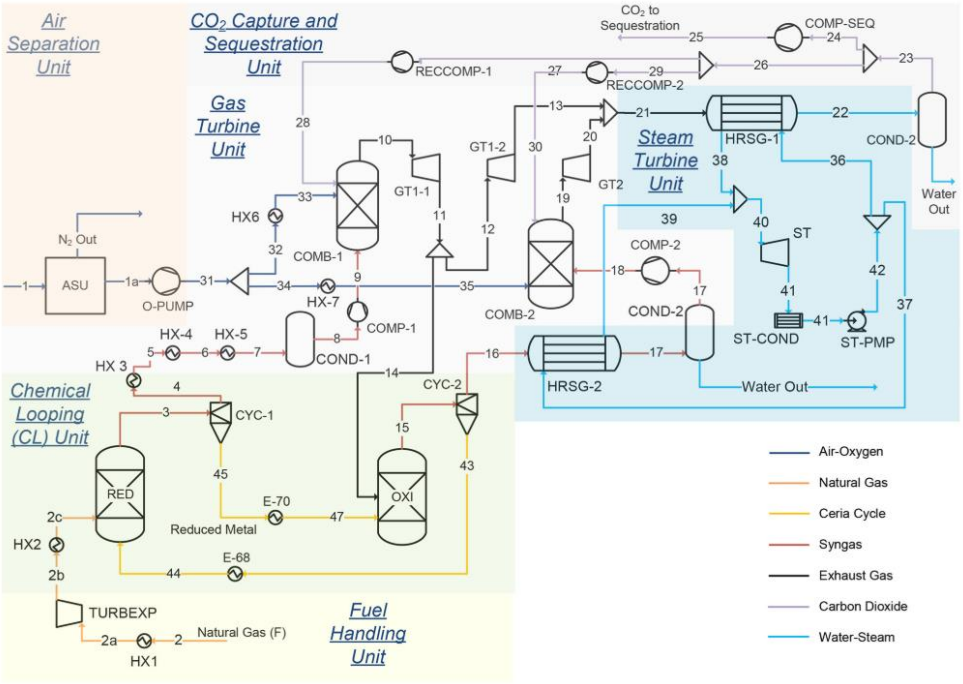


Fig. 21. Process simulation flowsheet of OXY−CC-CL unit [129], "Adapted with permission, Copyright (2018) Elsevier BV".

Nazir et al. [130] investigated a CLR unit integrated with a combined cycle power plant. A nickel-based OC was used and the plant was operated at 18 bar pressure. In this work, the syngas produced in the CLR unit was subjected to water gas shift reaction before capturing the $CO_2$ in a methyl diethanolamine capture system (MDEA). The outlet stream mostly consisting of hydrogen was compressed and preheated before burning in the gas turbine. Subsequently, the exhaust gas heat is recovered in a steam cycle. A comprehensive sensitivity study reported that the net electrical efficiencies ranged between 40 - 43.4% while the LCOE varied between 132.7 and 145.9 $/MWh.

In another study Nazir et al. [131] investigated a novel reactor concept called as gas switching reforming (GSR) (Fig. 22) [146] (as discussed in section (3.1.2)). Contrary to the chemical looping approach, in this concept, the OC was confined to one reactor with alternate switching of the feed gas to compete the GSR cycle. The reactor was operated at pressurized conditions of 18 bar at different OC utilization levels and steam to carbon ratios. It was also reported that

by eliminating the WGS step the efficiency and the LCOE can be improved considerably by ~1%-points and 3% reduction, respectively.

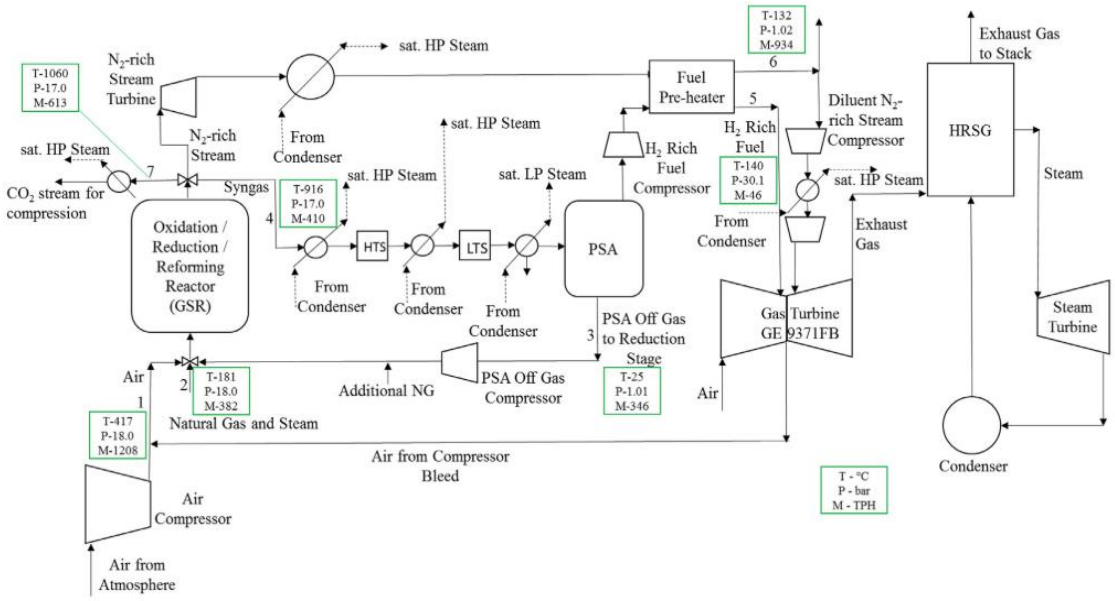


Fig. 22. Schematic of a GSR-CC process [131], "Adapted with permission, Copyright (2018) Elsevier BV".

The ability of GSR to efficiently integrate a PSA unit for pure $H_2$ production is an important advantage that can be exploited for flexible operation to balance variable renewable energy (VRE). When VRE output is low, the plant is operated as outlined above to produce power with $CO_2$ capture. However, when VRE output is high, the power cycle is deactivated and pure $H_2$ is exported instead. This allows most of the plant capital (the GSR reactors, WGS reactors, PSA unit and $CO_2$ compressors) as well as the downstream $CO_2$ transport and storage infrastructure to operate continuously, while variable electricity output is provided to balance VRE and $H_2$ is produced to decarbonize other sectors of the economy. A recent work [148] showed that such flexible power and $H_2$ production can strongly improve the economic performance of GSR-CC when operating as a mid-load plant to balance VRE. Even though the LCOE of GSR-CC was similar to an NGCC plant with post-combustion $CO_2$ capture under baseload conditions, a 5% better annualized investment return was calculated under mid-load

conditions. This conclusion was subsequently confirmed in a power system simulation study [149] showing that flexible GSR can reduce total power system costs by 8% and emissions by 41 kg/MWh, while increasing the optimal share of variable renewables by 50% relative to a system with conventional CCS plants. The GSR scenario also supplied a large amount of clean hydrogen to decarbonize sectors other than electricity. Such a flexible power and hydrogen plant would also be possible using coal or biomass as fuel, offering greater fuel flexibility to the power system. A coal-fired flexible power and hydrogen configuration was recently evaluated, showing that electric efficiencies exceeding 50% are possible with almost complete $CO_2$ capture [150]. Future economic and system-scale assessments are necessary to confirm the potential of this configuration to reduce energy system costs and emissions.

When deployed as a dedicated hydrogen production facility, GSR also holds great promise. Nazir et al. [151] showed how the hydrogen production efficiency can be optimized with respect to process pressure and further improved using added thermal mass (metal rods) in the reactor to limit temperature variations across the cycle. This work was subsequently extended to include an economic assessment [132], showing that GSR can produce clean hydrogen for a $CO_2$ avoidance cost as low as $15/ton. A promising commercialization pathway was also proposed where GSR plants are first constructed without $CO_2$ capture by expanding and venting the concentrated $CO_2$ stream, in which case produced hydrogen is cheaper than conventional SMR, and easily retrofitted for almost complete $CO_2$ avoidance when $CO_2$ prices rise and $CO_2$ transport and storage networks become available.

Gas switching reforming has also been studied for hydrogen generation using membranes for hydrogen extraction. Wassie et al. [133] combined the GSR reactor concept with the $H_2$ perm-selective membranes (MA-GSR). Given the intermittent nature of the GSR concept, a cluster of five reactors operated at 50 bar was considered undergoing cycles consisting of oxidation, reduction and reforming stages. The Pd-based membranes were inserted in each of the reactors

in the cluster. The membranes are expected to work only in the reforming stage, causing a relatively low utilization rate that negatively affects process economic performance.

This work was inspired by Spallina et al. [134] who performed a techno-economic assessment of a membrane-based chemical looping reforming (MA-CLR) plant integrated with $CO_2$ capture (Fig. 23). The plant was operated at different pressures ranging from 32-50 bar. Simultaneous OC reduction and methane reforming to syngas occur in the fuel reactor, while the hydrogen produced is continuously extracted by the Pd-membranes. The results showed that the $H_2$ yield by this configuration is about 20% higher than the conventional plants. This plant also offers low energy cost for $CO_2$ separation and compression which makes the overall reforming efficiency up to 20% higher than the conventional FTR (fired tubular reforming) with $CO_2$ scrubbing.

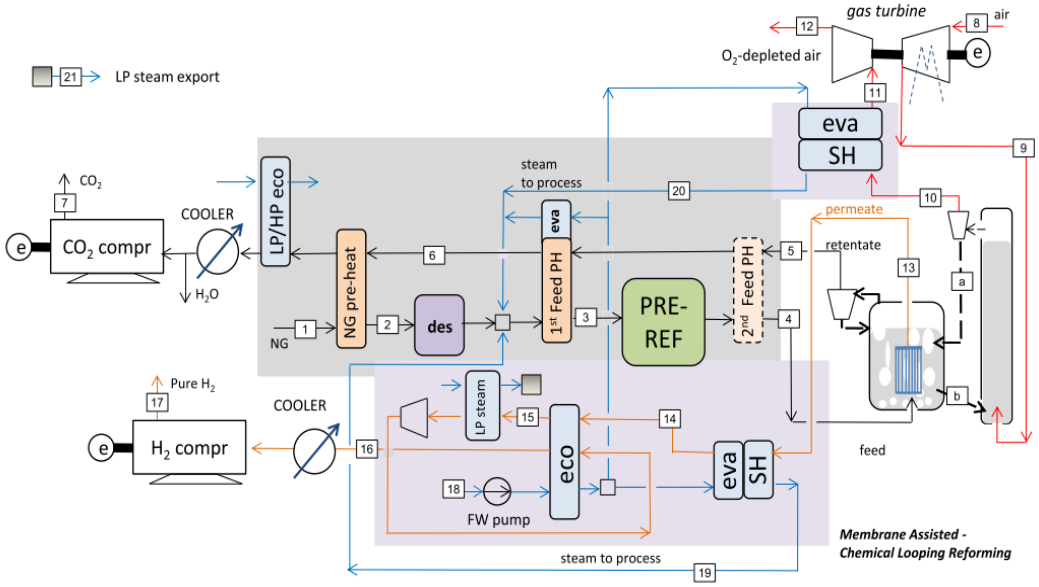


Fig. 23. Plant layout considered for the MA-CLR [134].

Prior to that study, Spallina et al. [135] carried out as similar study on CLR system. The process flow schematic shown in Fig. 24 consisted of a FR operating at 20 bar pressure. An increase in hydrogen efficiency by 8%-points and a slight reduction in LCOH was reported when compared to SMR plant with $CO_2$ capture. The lower efficiency was due to the lower hydrogen

yield and higher electric power consumption. The critical challenge in this configuration was the operation of dual fluidized bed reactors at elevated pressures.

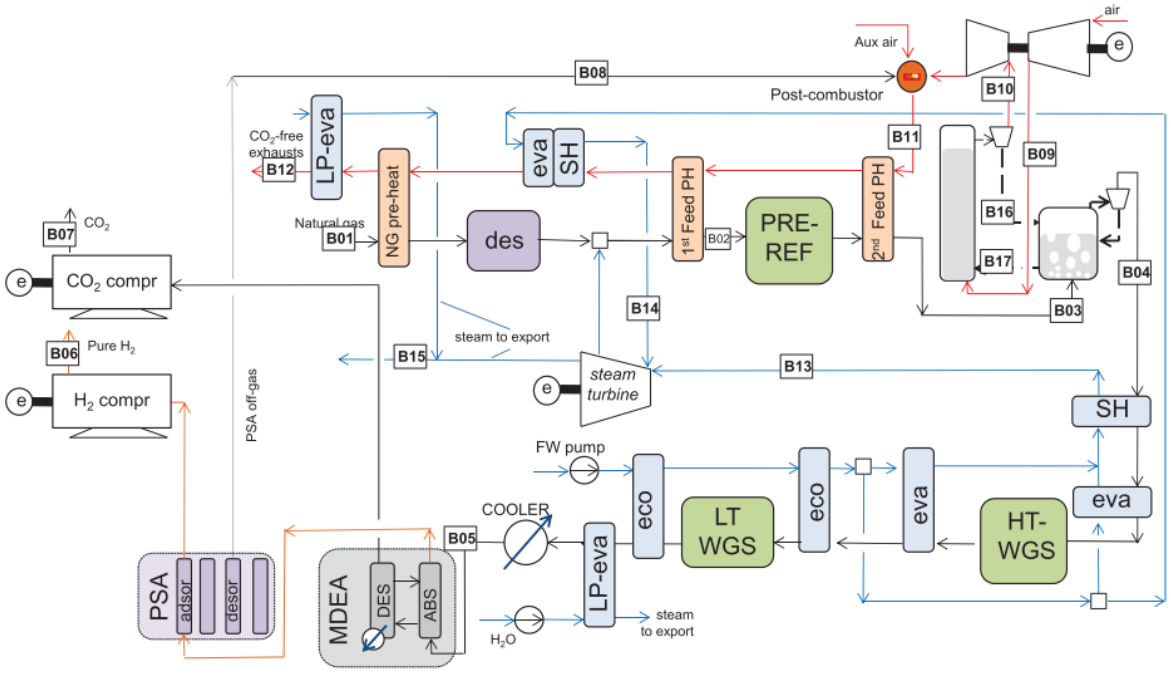


Fig. 24. Process simulation flowsheet of chemical looping reforming [135], "Adapted with permission, Copyright (2019) Elsevier BV".

Cloete et al. [136] proposed an alternative to the (MA-CLR) system studied by Spallina et al. [134]. The so-called membrane-assisted autothermal reforming (MA-ATR) consisted of an ASU providing oxygen to the reduced OC, replacing the air reactor of MA-CLR (Fig. 25). This was to avoid the challenge of maintaining reliable solids circulation between the air and fuel reactors at large scale under the very high pressures (50 bar or higher) required to maximize process efficiency. The very high operating pressure also means that the energy penalty of the ASU may not be so large compared to the losses involved in the compression and expansion of air to feed the MA-CLR air reactor. The economic assessment showed that hydrogen production by MA-ATR is only 1.5% more expensive than MA-CLR, which could be attractive given the significant process simplification. The cost of hydrogen production was lower than the MA-CLR plant discussed earlier mainly because of lower assumed natural gas prices. The

MA-ATR concept was also evaluated for ammonia production [152], capitalizing on the possibility to feed $N_2$ from the ASU as a sweep gas through the membranes to increase the achievable permeate pressure, thus reducing downstream compression work before the ammonia synthesis loop. This process configuration returned 11% lower ammonia costs than the conventional benchmark process without $CO_2$ capture.

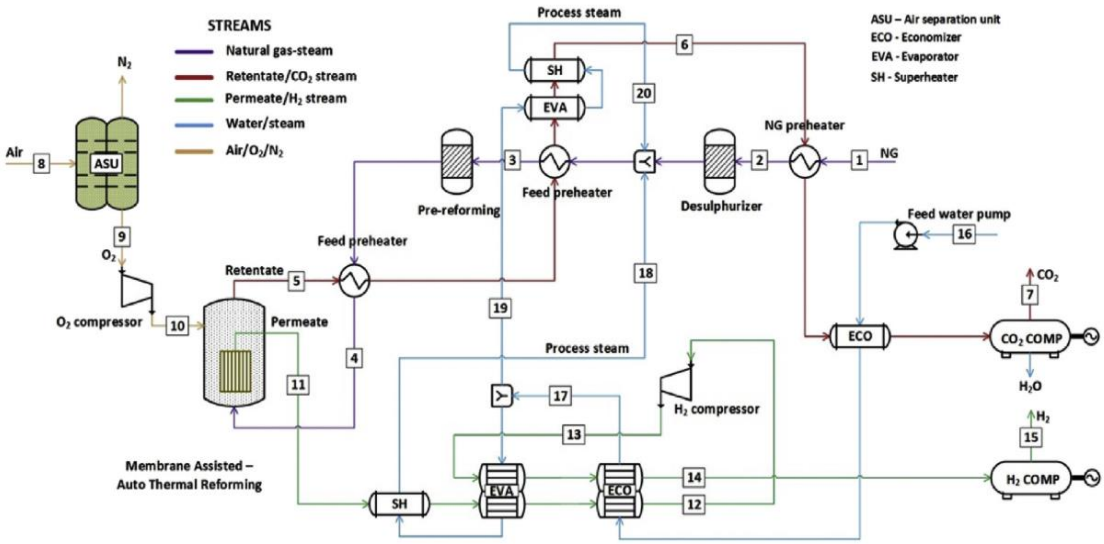


Fig. 25. Schematic of membrane assisted autothermal reforming plant [136], "Adapted with permission, Copyright (2019) Elsevier BV".

Pressurized chemical looping process in packed bed reactors was also used for ammonia production by Pereira et al. [153]. A three packed-beds (each for oxidation, reduction and reforming) were operated at pressure above 30 bar. The ammonia yield reported was ~1.9% more than the reference ammonia synthesis plant with $CO_2$ capture and with equally more equivalent specific energy consumption. The total plant cost was reduced by 19% owing to the pressurized reforming unit and $CO_2$ separation. The ammonia production cost estimated was ~5% less than the reference plant with negative $CO_2$ avoidance cost (-5 $/ton$_{CO2}$). A similar setup of three dynamically operated packed-bed reactors was also used for methanol production by Spallina et al. [154]. In this process, the reactors were operated at a pressure above 25 bar. An autothermal reforming process for syngas production was assumed as a reference plant

without $CO_2$ capture. The equivalent methanol production efficiency for the CL plant was slightly less than the reference plant (~0.5%-points). The methanol production costs estimated was 17% lower than the reference plant with negative $CO_2$ avoidance costs (-303 $/ton$_{CO2}$); due to significantly lower investment costs associated with CL plant.

### 4.3. Chemical looping water splitting

In the chemical looping water splitting process, steam is split into hydrogen and oxygen that oxidizes the OC. A concept involving three reactors, basically combining the chemical looping combustion and chemical looping water splitting processes is called a three-reactor chemical looping hydrogen (CLH) production. Khan and Shamim [137] referred to the process as reforming due to similarity of the overall reaction to the SMR process after the oxidation of the carbon monoxide to $CO_2$. However, this is misleading and should be referred to as water splitting. The configuration consisted of three reactors: the fuel reactor where the natural gas was converted into $CO_2$ and $H_2O$, the steam reactor where the water was split into $H_2$, and the air reactor where the reduced OC was re-oxidized. Iron-based OCs were used in the plant operated at 20 bar. Heat was recovered from the three outlet streams for power generation using a complex network of heat exchangers. The cost of hydrogen production reported was significantly lower compared to the case of SMR with $CO_2$ capture (about 2.7 $/kg). In a similar study, Khan and Shamim [138] compared the performance of a similar plant using an iron-based and tungsten-based OCs (Fig. 26). It was reported that the tungsten-based plant performed 4%-points better than the iron-based plant in terms of hydrogen production efficiency. As W-based oxides have a higher oxygen potential, they tend to absorb more oxygen when reacting with steam, consequently, producing more $H_2$, but the high cost of tungsten makes these OCs unaffordable. However, it was also reported that if the very high cost of tungsten-based OC were to be equal to that of the iron-based carrier, then the cost of

hydrogen production would come down to 1.5 $/kg. Although the price of a tungsten OC can never approach that of an iron OC, this result indicates the ultimate potential of developing a cheap OC with similar characteristics to the tungsten OC.

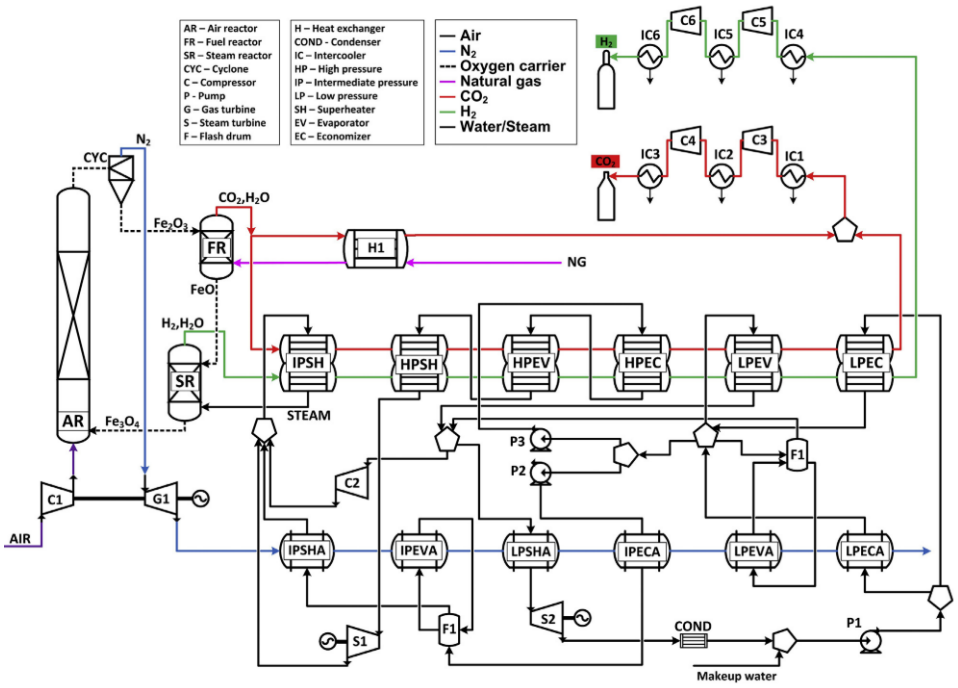


Fig. 26. Process flow diagram of TRCLR plant [138], "Adapted with permission, Copyright (2019) Elsevier BV".

Xiang and Zhou [140] proposed a process design which comprises of CLH generation unit which utilizes coke oven gas as the fuel and iron-based OC (Fig. 27). Part of the hydrogen produced was synthesized with nitrogen from an ASU to produce ammonia. In another configuration, a PSA unit was used to extract hydrogen from the coke oven gas before introducing it into the CLH unit. This ensured an increase in hydrogen production and also offered flexibility in the production of both hydrogen and ammonia depending on the market demand. The CLH unit was operated at 10 bar and was integrated as a mean of hydrogen source for the ammonia production, which was mostly used in the production of fertilizers. The results indicated that it was more efficient $H_2$ source than a conventional SMR.

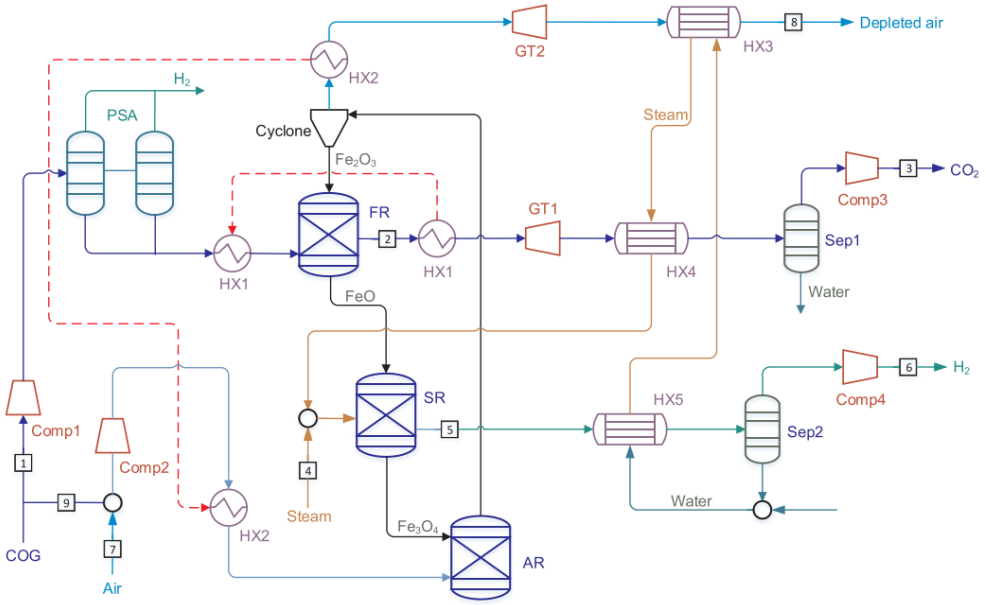


Fig. 27. Process diagram of the $CG_{PSA}$-CLH1 [140], "Adapted with permission, Copyright (2018) Elsevier BV".

## 4.4. Discussion of techno-economic assessment findings

The primary finding from this review of techno-economic assessment studies is that pressurized chemical looping processes are more attractive for hydrogen (or other chemicals) production than power production. This is because the maximum chemical looping reactor temperature severely constrains combined power cycle efficiency relative to modern NGCC plants with very high TIT, but good reforming efficiency can still be achieved at achievable reactor temperatures.

This reactor temperature limitation can be mitigated in CLC combined cycle plants by using an additional combustor after the CLC reactor or by firing the combined power cycle with hydrogen produced via CLR. However, both options impose significant added costs or emissions. In the case of added firing, emissions are introduced if natural gas is used and costs are increased if hydrogen is used. In the case of a hydrogen-fired combined cycle, the conversion losses in the reforming process are augmented by the additional conversion losses

in the combined cycle. Such strategies can still achieve reasonable techno-economic performance, but the superiority relative to benchmark post-combustion solutions is marginal.

For hydrogen production, on the other hand, the most efficient chemical looping configurations can approach the techno-economic performance of benchmark processes without any $CO_2$ capture, easily outperforming conventional $CO_2$ capture benchmarks. Several promising pathways exist, each with unique advantages relative to the conventional steam methane reforming hydrogen production pathway. For GSR, the perfect heat transfer of the combustion heat to the reforming reaction via the oxygen carrier material allows the reforming to be completed at higher temperatures, leading to good methane conversion at lower S/C ratios. This reduces the heat required to raise steam, improving efficiency. For membrane-assisted reforming and water splitting, the downstream hydrogen separation processes are avoided, saving significant capital costs and efficiency losses. All three of these hydrogen production pathways show great promise to produce hydrogen and other chemicals with minimal or even negative $CO_2$ avoidance costs.

Finally, emerging studies of flexible power and hydrogen production plants for balancing variable renewable energy shows promise, given the large momentum behind wind and solar power and the hydrogen economy. Such processes capitalize on the high attractiveness of chemical looping for hydrogen production, while concentrating power production only during times of high electricity prices (low wind and solar output) to compensate for the marginal competitiveness of combustion discussed earlier.

## 5. Pressurized calcium looping process

Calcium looping (CaL) is a promising energy efficient $CO_2$ capture technology. It is largely applied as a post combustion technology for capturing $CO_2$ from the flue gas following an

equilibrium reaction between calcium oxide and $CO_2$ to form calcium carbonate ($CaO + CO_2 \rightarrow CaCO_3$). At atmospheric pressure, the carbonation takes place at temperatures of ~700°C while the regeneration takes place above 900°C. Most of post combustion studies have been completed at atmospheric pressure demonstrating the technology up to TRL6. Abanades et al. [155] provides a good overview on the technology development up to 2015 building up on previous reviews from Harrison in 2008 [156] (focused on applying CaL in for sorbent enhanced hydrogen production) and Anthony et al. in 2011 [157] for CaL technology in general.

Pressurized operation of this technology can bring several advantages to the carbonation reaction such as improved kinetics, shifting the equilibrium in a positive direction and enhanced hydrodynamics and heat/mass transfer rates [158]. However, it makes the regeneration challenging, negatively affecting the equilibrium, and requiring temperatures beyond 1000°C to achieve satisfying conversion rates. Abanades et al. [155] identified this as the key challenge to solve to unlock the full potential of CaL technology when targeting pressurized pre-combustion for production of an $H_2$ rich gas stream in methane reforming or gasification of biomass (or coal) intensified by $CO_2$ adsorption on CaO.

Most of recent studies continued focusing on the positive effect of pressure on CaO enhanced hydrogen production. CaO was reported to enhance the selectivity to hydrogen in coal [159] and biomass gasification [160]. High pressure operation using CaO was applied to In-situ biomass combustion and has shown to successfully reduce tar yield [160]. Gas–solid trickle flow reactor packed experiments have shown that hydrogen rich flue gas could be produced using sorbent enhanced SMR at temperatures as low as 500-600°C and a pressure of 4 bar [161].

Other studies focused on optimizing the carbonation reaction attempting to enhance the kinetics in specific applications. Steam addition was found to promote $CO_2$ adsorption via the formation

of surface OH groups on the CaO surface [162]. $K_2CO_3$ catalyst addition was found to significantly improve coal gasification reactivity while the CaO sorbent mainly played the role of $CO_2$ absorbent and heat carrier [163]. The same study has reported that the reaction heat calculation results indicated that the catalytic calcium looping hydrogen generation process could shift from endothermic to exothermic as the pressure increases beyond 2.0 MPa.

An interesting alternative technology based on CaL for decarbonizing natural gas to hydrogen with integrated $CO_2$ capture is the Ca-Cu process. This technology uses the heat generated from the exothermic reaction of Cu-based oxygen carrier reduction to regenerate the $CaCO_3$ sorbent [139]. Methane reforming occurs similarly to the sorbent enhanced methane reforming process where the produced $CO_2$ adsorbs on the CaO sorbent shifting the equilibrium reaction for maximizing conversion to $H_2$ (the WGS reaction occurs simultaneously yielding to high purity $H_2$ after $CO_2$ removal by the sorbent). This process is receiving increased interest due to the predicted high energy efficiency and lower product costs compared to benchmarking $CO_2$ capture technologies [164]. Experimental development studies were completed, mainly focusing on the Ca-Cu material and its performance, testing under the main critical step of the process which combines reduction of CuO and calcination $CaCO_3$ [165–167]. A recent review by Fernández et al. [168] on the technology provides a complete overview of the progress both on process development, modelling and integration.

CaL technology was also applied for intensifying the Water-Gas-Shift reaction (WGS) through removing the produced $CO_2$ in the process using the calcium-based sorbent. The process is known as sorbent enhanced water-gas-shift (SEWGS). A recent study on this process has demonstrated the possibility of experimentally achieving high-purity $H_2$ (99.4% in dry basis) in the SEWGS process at 573 K, 12 atm and an initial $H_2O$/CO molar ratio of 1.5 with a three catalyst/sorbent layered configuration [169]. Another study combined WGS Cu-based catalyst and K-doped hydrotalcite for $CO_2$ capture in the SEWGS process at different pressures. It has

been shown that if steam is used during the regeneration step, all sites can be effectively regenerated, achieving a stable working sorption capacity [170].

## 6. Conclusion and Outlook

This paper reviews pressurized chemical looping studies addressing the different aspects that affect reactor performance, the different reactor configurations proposed, and the costs of $CO_2$ capture at elevated pressure. The effect of pressure on the thermodynamic equilibrium depends on the reactions involved in the process, governed by Le Chatelier's principle. As for the kinetics, the pressure was found to negatively affect the reaction rate when the partial pressure of the fuel is maintained constant, which was attributed to the increase in the external mass transfer resistance. At constant fuel molar fraction, contradicting findings were reported showing both negative and positive effects of the pressure on the reaction rate. Results suggest that keeping the gas space velocity constant counteracted the negative effect of the external mass transfer resistance. Pressurized reactor experimental results confirm this interpretation. This implies that the negative effect of pressure on kinetics in real reactors could be much smaller than suggested by most TGA studies, making pressurization an effective pathway for process intensification of chemical looping processes. This is an important finding for the future of pressurized chemical looping because the ability to leverage high reaction rates for downsizing pressurized reactors is important for controlling capital costs. The effect of pressure on the oxygen carrier morphology and durability is not widely studied yet; therefore, we highly recommend future research in this important aspect to assess the durability of various oxygen carriers at elevated pressure conditions.

A limited number of studies have been reported on experimental testing of reactor configurations under pressurized conditions, distributed between gas switching both under fluidized and packed bed modes (for gaseous fuel), interconnected fluidized bed reactors

(mainly for solid fuel), and moving bed reactors (for the steam-iron process). All pressurized demonstration studies remain at lab and pre-pilot scales (up to 50 $kW_{th}$ capacity). A summarized comparison of six different reactor configurations is also presented. Relative to the conventional dual fluidized bed chemical looping reactor configuration, several concepts are available to simplify operation under pressurized conditions, although these involve trade-offs with respect to reactor footprint, thermochemical stresses on the oxygen carrier, and $CO_2$ capture ratio.

Techno-economic assessment studies on pressurized chemical looping have reported a wide range of energy penalties and associated $CO_2$ avoidance costs for different chemical looping processes, reactor configurations and process integrations. The wide variation in the assumptions employed hampers direct comparisons between studies, but most benchmarking works reported that chemical looping outperforms conventional $CO_2$ capture processes. Pressurized CLC faces a fundamental challenge from the maximum achievable reactor temperature that is far below the firing temperature of modern gas turbines. Recent works have proposed added firing after the CLC reactors to mitigate this challenge. Other chemical looping processes are not hampered by this limitation. In particular, hydrogen production concepts based on chemical looping reforming and chemical looping water splitting promise techno-economic performance approaching benchmarks without any $CO_2$ capture. Another important aspect recently studied is flexible power output to balance variable renewable energy, either through energy storage in the oxygen carrier or flexible output of power and hydrogen. Large energy system benefits have been found for the flexible power and hydrogen pathway.

The promising results from the techno-economic assessment studies present a strong case for further experimental demonstration of the promising chemical looping technologies in the reactor configurations that were identified to be suitable for pressurized operation. Thorough testing of these reactor configurations at operating temperatures and pressures relevant to

industrial conditions for the specific processes is needed to identify and solve the technical challenges hindering their successful and safe operation with good performance in terms of fuel conversion and separation efficiency. Once demonstrated under these conditions, reactor concepts designed especially for pressurized operation should be relatively simple to scale up for commercialization, allowing chemical looping technology to accelerate the global energy transition via clean power, hydrogen and system flexibility.

## Nomenclature

| **Acronyms** | |
|---|---|
| AR | Air reactor |
| ASU | Air separation unit |
| CCUS | Carbon Capture, Utilization and Storage |
| CGSM | Changing Grain Size Model |
| CLC | Chemical looping combustion |
| CLH | Chemical looping hydrogen |
| CLR | Chemical looping reforming |
| CLAS | Chemical looping air separation |
| CLOP | Chemical looping oxygen production |
| CLOU | Chemical looping with oxygen uncoupling |
| CFB | Circulating fluidized-bed |
| FR | Fuel reactor |
| FTR | Fired tubular reforming |
| GSR | Gas switching reforming |
| HAT | Humid air turbine |
| ICR | Internally circulating reactor |
| IGCC | Integrated gasification combined cycle |
| OC | Oxygen carrier |
| LHV | Lower heating value |
| LCOE | Levelized Cost of Electricity |
| LCOH | Levelized Cost of Hydrogen |
| MA-ATR | Membrane-Assisted Autothermal Reforming |
| MA-CLR | Membrane-Assisted Chemical looping reforming |
| MA-GSR | Membrane-Assisted Gas Switching Reforming |
| MDEA | Methyl diethanolamine |
| MSB | Magnetic suspension balance |
| NGCC | Natural Gas Fired Combined Cycle |
| OXY-CC | Oxyfuel combined cycle |
| PCLC | Pressurized Chemical looping combustion |
| PSD | Particle size distribution |
| PTGA | Pressurized thermogravimetric analysis |
| SCL | Syngas chemical looping |
| TGA | Thermogravimetric Analysis |
| TIT | Turbine inlet temperature |
| TRL | Technology readiness level |

| | |
|---|---|
| VRE | Variable renewable energy |
| WGS | Water gas shift |
| **Symbols** | |
| A | pre-exponential factor ($s^{-1}$) |
| b | stoichiometric factor, mol of solid reacting (mol of gas)$^{-1}$ |
| C | gas concentration, mol $m^{-3}$ |
| $C_{eq}$ | gas concentration at equilibrium conditions, mol $m^{-3}$ |
| $C_{CO,b}$ | The concentration of CO at the surface of the particle, mol $m^{-3}$ |
| D | diffusivity, $m^2/s$ |
| d | Fitted parameter for pressurized kinetics |
| E | activation energy, J $mol^{-1}$ |
| $\Delta G$ | Gibbs free energy |
| $\Delta H$ | reaction enthalpy (kJ/mol) |
| $k_0$ | pre-exponential factor of the chemical reaction rate constant, $mol^{1-n}$ $m^{3n-2}$ $s^{-1}$ |
| $k_{0,P}$ | pre-exponential factor of the chemical reaction rate constant for pressurized conditions, $mol^{1-n}$ $m^{3n-2}$ $s^{-1}$ |
| k | chemical reaction rate constant, $mol^{1-n}$ $m^{3n-2}$ $s^{-1}$ |
| k' | The overall rate constant, $m^3/(g\ s)$ |
| L | layer thickness of the reacting solid for the platelike geometry, m |
| M | Molecular weight |
| m | mass of sample, g |
| $m_{ox}$ | mass of the fully oxidized oxygen carrier, g |
| n | reaction order |
| P | total pressure, atm |
| $P_p$ | partial pressure, atm |
| $P_G$ | partial pressure of reacting gas G |
| $P_T$ | Total pressure |
| R | ideal gas constant, J $mol^{-1}$ $K^{-1}$ |
| $R_0$ | oxygen transport capacity of the oxygen carrier |
| r | grain radius, m |
| S | specific surface area of the particle |
| $S_o$ | The initial reaction surface area, $m^{-1}$ |
| t | time, s |
| T | Temperature, K |
| u | Fluidization velocity (m/s) |
| $u_{mf}$ | Minimum fluidizing velocity (m/s) |
| X | solid conversion |
| w | mass fraction, kg/kg |
| **Greek letters** | |
| $\rho_m$ | Molar density of the reacting material, mol $m^{-3}$ |
| $\tau$ | Time for complete solid conversion, s |
| $\varepsilon$ | Porosity, $m^3/m^3$ |
| $\varepsilon_{mf}$ | Porosity at minimal fluidizing velocity, $m^3/m^3$ |
| $\varepsilon_{mb}$ | Porosity at minimal bubbling velocity, $m^3/m^3$ |
| $\psi$ | Structure parameter (calculated from pore structure measurements and BET surface area) |

## Acknowledgement

The authors would like to acknowledge the financial support of the Research Council of Norway under the CLIMIT program (project number: 255462). The authors also acknowledge the financial support for the ERA-NET ACT GaSTech Project, co-funded by the Research Council of Norway and the European Commission under the Horizon 2020 program, ACT Grant Agreement No. 691712.

## References

[1] V. Masson-Delmotte, P. Zhai, H.-O. Pörtner, D. Roberts, J. Skea, P.R. Shukla, A. Pirani, W. Moufouma-Okia, C. Péan, R. Pidcock, S. Connors, J.B.R. Matthews, Y. Chen, X. Zhou, M.I. Gomis, E. Lonnoy, T. Maycock, M. Tignor, T. Waterfield, An IPCC Special Report on the impacts of global warming of 1.5°C above pre-industrial levels and related global greenhouse gas emission pathways, in the context of strengthening the global response to the threat of climate change, sustainable development, 2018.

[2] M. Bui, C.S. Adjiman, A. Bardow, E.J. Anthony, A. Boston, S. Brown, P.S. Fennell, S. Fuss, A. Galindo, L.A. Hackett, J.P. Hallett, H.J. Herzog, G. Jackson, J. Kemper, S. Krevor, G.C. Maitland, M. Matuszewski, I.S. Metcalfe, C. Petit, G. Puxty, J. Reimer, D.M. Reiner, E.S. Rubin, S.A. Scott, N. Shah, B. Smit, J.P.M. Trusler, P. Webley, J. Wilcox, N. Mac Dowell, Carbon capture and storage (CCS): the way forward, Energy Environ. Sci. 11 (2018) 1062–1176.

[3] E.S. Rubin, J.E. Davison, H.J. Herzog, The cost of CO2 capture and storage, Int. J. Greenh. Gas Control. 40 (2015) 378–400.

[4] M. Ishida, D. Zheng, T. Akehata, Evaluation of a chemical-looping- combustion power-generation system by graphic exergy analysis, Energy. 12 (1987) 147–154.

[5] M. Ryden, A. Lyngfelt, T. Mattisson, Synthesis gas generation by chemical-looping reforming in a continuously operating laboratory reactor, Fuel. 85 (2006) 1631–1641.

[6] T. Pröll, J. Bolhàr-Nordenkampf, P. Kolbitsch, H. Hofbauer, Syngas and a separate nitrogen/argon stream via chemical looping reforming – A 140 kW pilot plant study, Fuel. 89 (2010) 1249–1256.

[7] M. Ortiz, L.F. de Diego, A. Abad, F. García-Labiano, P. Gayá, J. Adá Nez, P. Gayán, J. Adánez, Hydrogen production by auto-thermal chemical-looping reforming in a pressurized fluidized bed reactor using Ni-based oxygen carriers, Int. J. Hydrogen Energy. 35 (2010) 151–160.

[8] M. Rydén, M. Arjmand, Continuous hydrogen production via the steam–iron reaction by chemical looping in a circulating fluidized-bed reactor, Int. J. Hydrogen Energy. 37 (2012) 4843–4854.

[9] L.F. Wang, S.Z. Wang, M. Luo, Review of Hydrogen Production from the Steam-Iron Process by Chemical-Looping Combustion, Adv. Mater. Res. 953–954 (2014) 966–969.

[10] P. Chiesa, G. Lozza, A. Malandrino, M. Romano, V. Piccolo, Three-reactors chemical looping process for hydrogen production, Int. J. Hydrogen Energy. 33 (2008) 2233–2245.

[11] L.F. De Diego, M. Ortiz, F. García-Labiano, J. Adánez, A. Abad, P. Gayán, Hydrogen production by chemical-looping reforming in a circulating fluidized bed reactor using Ni-based oxygen carriers, J. Power Sources. 192 (2009) 27–34.

[12] S. Cloete, A. Giuffrida, M. Romano, P. Chiesa, M. Pishahang, Y. Larring, Integration of chemical looping oxygen production and chemical looping combustion in integrated gasification combined cycles, Fuel. 220 (2018) 725–743.

[13] B. Moghtaderi, Application of Chemical Looping Concept for Air Separation at High Temperatures †, Energy & Fuels. 24 (2010) 190–198.

[14] J. Adánez, A. Abad, Chemical-looping combustion: Status and research needs, Proc. Combust. Inst. 37 (2019) 4303–4317.

[15] T. Mattisson, M. Keller, C. Linderholm, P. Moldenhauer, M. Rydén, H. Leion, A. Lyngfelt, Chemical-looping technologies using circulating fluidized bed systems: Status of development, Fuel Process. Technol. 172 (2018) 1–12.

[16] A. Lyngfelt, A. Brink, Ø. Langørgen, T. Mattisson, M. Rydén, C. Linderholm, 11,000 h of chemical-looping combustion operation—Where are we and where do we want to go?, Int. J. Greenh. Gas Control. 88 (2019) 38–56.

[17] X. Zhu, Q. Imtiaz, F. Donat, C.R. Mü, F. Li, Chemical looping beyond combustion-a perspective, (2020).

[18] H.M. Kvamsdal, K. Jordal, O. Bolland, A quantitative comparison of gas turbine cycles with CO 2 capture, Energy. 32 (2007) 10–24.

[19] J. Wolf, M. Anheden, J. Yan, Comparison of nickel- and iron-based oxygen carriers in chemical looping combustion for CO capture in power generation, Fuel. 84 (2005) 993–1006.

[20] V. Subramani, P. Sharma, L. Zhang, K. Liu, Catalytic Steam Reforming Technology for the Production of Hydrogen and Syngas, in: Hydrog. Syngas Prod. Purif. Technol., John Wiley & Sons, Inc., Hoboken, NJ, USA, 2009: pp. 14–126.

[21] F. García-Labiano, J. Adánez, L.F. de Diego, P. Gayán, A. Abad, Effect of Pressure on the Behavior of Copper-, Iron-, and Nickel-Based Oxygen Carriers for Chemical-Looping Combustion, Energy & Fuels. 20 (2006) 26–33.

[22] A. Abad, F. García-Labiano, L.F. de Diego, P. Gayán, J. Adánez, Reduction Kinetics of Cu-, Ni-, and Fe-Based Oxygen Carriers Using Syngas (CO + H 2 ) for Chemical-Looping Combustion, Energy & Fuels. 21 (2007) 1843–1853.

[23] R. Siriwardane, J. Poston, K. Chaudhari, A. Zinn, T. Simonyi, C. Robinson, Chemical-Looping Combustion of Simulated Synthesis Gas Using Nickel Oxide Oxygen Carrier Supported on Bentonite, Energy & Fuels. 21 (2007) 1582–1591.

[24] H. Gu, L. Shen, J. Xiao, S. Zhang, T. Song, D. Chen, Evaluation of the Effect of Sulfur on Iron-Ore Oxygen Carrier in Chemical-Looping Combustion, Ind. Eng. Chem. Res. 52 (2013) 1795–1805.

[25] S. Zhang, R. Xiao, W. Zheng, Comparative study between fluidized-bed and fixed-bed operation modes in pressurized chemical looping combustion of coal, Appl. Energy. 130 (2014) 181–189.

[26] S. Luo, L. Zeng, D. Xu, M. Kathe, E. Chung, N. Deshpande, L. Qin, A. Majumder, T.-L. Hsieh, A. Tong, Z. Sun, L.-S. Fan, Shale gas-to-syngas chemical looping process for stable shale gas conversion to high purity syngas with a H 2 : CO ratio of 2 : 1, Energy Environ. Sci. 7 (2014) 4104–4117.

[27] H.P. Hamers, F. Gallucci, G. Williams, P.D. Cobden, M. van Sint Annaland, Reactivity of Oxygen Carriers for Chemical-Looping Combustion in Packed Bed Reactors under Pressurized Conditions, Energy & Fuels. 29 (2015) 2656–2663.

[28] N. Deshpande, A. Majumder, L. Qin, L.-S. Fan, High-Pressure Redox Behavior of Iron-Oxide-Based Oxygen Carriers for Syngas Generation from Methane, Energy & Fuels. 29 (2015) 1469–1478.

[29] X. Lu, R.A. Rahman, D.Y. Lu, F.N. Ridha, M.A. Duchesne, Y. Tan, R.W. Hughes, Pressurized chemical looping combustion with CO: Reduction reactivity and oxygen-transport capacity of ilmenite ore, Appl. Energy. 184 (2016) 132–139.

[30] M.A. San Pio, F. Gallucci, I. Roghair, M. van Sint Annaland, Gas-solids kinetics of CuO/Al2O3 as an oxygen carrier for high-pressure chemical looping processes: The influence of the total pressure, Int. J. Hydrogen Energy. 42 (2017) 12111–12121.

[31] Y. Tan, F.N. Ridha, D.Y. Lu, R.W. Hughes, Reduction Kinetics of Ilmenite Ore for Pressurized Chemical Looping Combustion of Simulated Natural Gas, Energy & Fuels. 31 (2017) 14201–14210.

[32] Y. Tan, F.N. Ridha, M.A. Duchesne, D.Y. Lu, R.W. Hughes, Reduction Kinetics of Ilmenite Ore as an Oxygen Carrier for Pressurized Chemical Looping Combustion of Methane, Energy & Fuels. 31 (2017) 7598−7605.

[33] L. Chen, L. Kong, J. Bao, M. Combs, H.S. Nikolic, Z. Fan, K. Liu, Experimental evaluations of solid-fueled pressurized chemical looping combustion – The effects of pressure, solid fuel and iron-based oxygen carriers, Appl. Energy. 195 (2017) 1012–1022.

[34] S. Rana, Z. Sun, P. Mehrani, R. Hughes, A. Macchi, Ilmenite oxidation kinetics for pressurized chemical looping combustion of natural gas, Appl. Energy. 238 (2019) 747–759.

[35] L. Díez-Martín, G. Grasa, R. Murillo, M. Martini, F. Gallucci, M. van Sint Annaland, Determination of the oxidation kinetics of high loaded CuO-based materials under suitable conditions for the Ca/Cu H2 production process, Fuel. 219 (2018) 76–87.

[36] F. García-Labiano, J. Adánez, A. Abad, L.F. de Diego, P. Gayán, Effect of Pressure on the Sulfidation of Calcined Calcium-Based Sorbents, Energy & Fuels. 18 (2004) 761–769.

[37] S.S. Chauk, R. Agnihotri, R.A. Jadhav, S.K. Misro, L.-S. Fan, Kinetics of high-pressure removal of hydrogen sulfide using calcium oxide powder, AIChE J. 46 (2000) 1157–1167.

[38] R. Agnihotri, S.S. Chauk, S.K. Misro, L.-S. Fan, High-Pressure Reaction Kinetics of Hydrogen Sulfide and Uncalcined Limestone Powder, Ind. Eng. Chem. Res. 38 (1999)

3802–3811.

[39] K. Qiu, O. Lindqvist, Direct sulfation of limestone at elevated pressures, Chem. Eng. Sci. 55 (2000) 3091–3100.

[40] K. Qiu, E.J. Anthony, L. Jia, Oxidation of sulfided limestone under the conditions of pressurized fluidized bed combustion, FUEL. 80 (2001) 549–558.

[41] F. Garcã A-Labiano, A. Abad, L.F. De Diego, P. Gayã, J. Adã Anez, Calcination of calcium-based sorbents at pressure in a broad range of CO2 concentrations, 2002.

[42] P. Basinas, Y. Wu, P. Grammelis, E.J. Anthony, J.R. Grace, C. Jim Lim, Effect of pressure and gas concentration on CO2 and SO2 capture performance of limestones, Fuel. 122 (2014) 236–246.

[43] D.H. Ahn, B.M. Gibbs, K.H. Ko, J.J. Kim, Gasification kinetics of an Indonesian sub-bituminous coal-char with CO2 at elevated pressure, Fuel. 80 (2001) 1651–1658.

[44] W.C. Hecker, P.M. Madsen, M.R. Sherman, J.W. Allen, R.J. Sawaya, T.H. Fletcher, High-Pressure Intrinsic Oxidation Kinetics of Two Coal Chars, Energy & Fuels. 17 (2003) 427–432.

[45] W.E.S.E.N.L. R. Byron Bird, Transport Phenomena, 2nd Edition, 2007.

[46] J.W. Butler, C. Jim Lim, J.R. Grace, Kinetics of CO2 absorption by CaO through pressure swing cycling, Fuel. 127 (2014) 78–87.

[47] K.S. Oberoi, J. Abbasian, Effects of External Factors on the Measurement of Gas-Solid Reaction Rates, (2004).

[48] M.A. Kibria, P. Sripada, S. Bhattacharya, Rational design of thermogravimetric experiments to determine intrinsic char gasification kinetics, Proc. Combust. Inst. 37 (2019) 3023–3031.

[49] X. Guo, G. Chang, X. Tan, X. Hu, Q. Guo, Kinetics of Coal Char Gasification with Fe-Based Oxygen Carriers under Pressured Conditions, (2020).

[50] Z. Zhang, J.G. Yao, M.E. Boot-Handford, P.S. Fennell, Pressurised chemical-looping combustion of an iron-based oxygen carrier: Reduction kinetic measurements and modelling, Fuel Process. Technol. 171 (2018) 205–214.

[51] R.C. Everson, H.W.J.P. Neomagus, R. Kaitano, The random pore model with intraparticle diffusion for the description of combustion of char particles derived from mineral- and inertinite rich coal, Fuel. 90 (2011) 2347–2352.

[52] J. Adanez, A. Abad, F. Garcia-Labiano, P. Gayan, L.F. de Diego, Progress in Chemical-Looping Combustion and Reforming technologies, Prog. Energy Combust. Sci. 38 (2012) 215–282.

[53] J. Li, J.A.M. Kuipers, Effect of pressure on gas–solid flow behavior in dense gas-fluidized beds: a discrete particle simulation study, Powder Technol. 127 (2002) 173–184.

[54] I. Sidorenko, M.J. Rhodes, Influence of pressure on fluidization properties, Powder Technol. 141 (2004) 137–154.

[55] M. Banaei, R. Dellaert, N.G. Deen, M. van Sint Annaland, J.A.M. Kuipers, Borescopy

in pressurized gas-solid fluidized beds, AIChE J. 64 (2018) 3303–3311.

[56] M.A. Cuenca, E.J. Anthony, Pressurized Fluidized Bed Combustion, Springer Netherlands, Dordrecht, 1995.

[57] P.E.G. Gogolek, J.R. Grace, Fundamental hydrodynamics related to pressurized fluidized bed combustion, Prog. Energy Combust. Sci. 21 (1995) 419–451.

[58] J. Shabanian, J. Chaouki, Effects of temperature, pressure, and interparticle forces on the hydrodynamics of a gas-solid fluidized bed, Chem. Eng. J. 313 (2017) 580–590.

[59] M. Alvarez Cuenca, E. J. Anthony, Pressurized Fluidized Bed Combustion, Springer Netherlands, Dordrecht, 1995.

[60] S. Wang, G. Wang, F. Jiang, M. Luo, H. Li, Chemical looping combustion of coke oven gas by using Fe2O3/CuO with MgAl2O4 as oxygen carrier, Energy Environ. Sci. 3 (2010) 1353–1360.

[61] R. Xiao, L. Chen, C. Saha, S. Zhang, S. Bhattacharya, Pressurized chemical-looping combustion of coal using an iron ore as oxygen carrier in a pilot-scale unit, Int. J. Greenh. Gas Control. 10 (2012) 363–373.

[62] R.W. Breault, Handbook of chemical looping technology, WILEY-VCH Verlag, 2018.

[63] H.-J. Ryu, D. Lee, S.-H. Jo, S.-Y. Lee, J.-I. Baek, Preliminary Test Results in a 0.5 MWth Pressurized Chemical Looping Combustor, in: 14th Int. Conf. Greenh. Gas Control Technol. GHGT-14, 2018.

[64] R.H. Emma Moreside, Robert Symonds, Dennis Lu, Reactor Design of CanmetENERGY's Pilot-Scale Pressurized Chemical Looping Conversion, in: Fluid. XVI, AIChE, 2019.

[65] A. Zaabout, S. Cloete, S. Amini, Autothermal operation of a pressurized Gas Switching Combustion with ilmenite ore, Int. J. Greenh. Gas Control. 63 (2017) 175–183.

[66] A. Zaabout, S. Cloete, J.R. Tolchard, S. Amini, A pressurized Gas Switching Combustion reactor: Autothermal operation with a CaMnO3−δ-based oxygen carrier, Chem. Eng. Res. Des. 137 (2018) 20–32.

[67] A. Zaabout, S. Cloete, S.T. Johansen, M. Van, S. Annaland, F. Gallucci, S. Amini, Experimental Demonstration of a Novel Gas Switching Combustion Reactor for Power Production with Integrated CO2 Capture, Ind. Eng. Chem. Res. 52 (2013) 14241−14250.

[68] S.A. Wassie, Membrane-assisted chemical switching reforming for pure hydrogen production with integrated CO2 capture, 2018.

[69] S. Cloete, A. Zaabout, M.C. Romano, P. Chiesa, G. Lozza, F. Gallucci, M. van Sint Annaland, S. Amini, Optimization of a Gas Switching Combustion process through advanced heat management strategies, Appl. Energy. 185 (2017) 1459–1470.

[70] A. Ugwu, A. Zaabout, J.R. Tolchard, P.I. Dahl, S. Amini, Gas Switching Reforming for syngas production with iron-based oxygen carrier-the performance under pressurized conditions, Int. J. Hydrogen Energy. 45 (2020) 1267–1282.

[71] A. Zaabout, P.I. Dahl, A. Ugwu, J.R. Tolchard, S. Cloete, S. Amini, Gas Switching Reforming (GSR) for syngas production with integrated CO2 capture using iron-based oxygen carriers, Int. J. Greenh. Gas Control. 81 (2019) 170–180.

[72] GaSTech - Demonstration of Gas Switching Technology for Accelerated Scale-up of Pressurized Chemical Looping Applications.

[73] S.A. Wassie, J.A. Medrano, A. Zaabout, S. Cloete, J. Melendez, D.A.P. Tanaka, S. Amini, M. van Sint Annaland, F. Gallucci, Hydrogen production with integrated CO2 capture in a membrane assisted gas switching reforming reactor: Proof-of-Concept, Int. J. Hydrogen Energy. 43 (2018) 6177–6190.

[74] S.A. Wassie, S. Cloete, V. Spallina, F. Gallucci, S. Amini, M. van Sint Annaland, Techno-economic assessment of membrane-assisted gas switching reforming for pure H2 production with CO2 capture, Int. J. Greenh. Gas Control. 72 (2018) 163–174.

[75] A. Zaabout, S. Cloete, S. Amini, Innovative Internally Circulating Reactor Concept for Chemical Looping-Based CO 2 Capture Processes: Hydrodynamic Investigation, Chem. Eng. Technol. 39 (2016) 1413–1424.

[76] M. Osman, A. Zaabout, S. Cloete, S. Amini, Internally circulating fluidized-bed reactor for syngas production using chemical looping reforming, Chem. Eng. J. 377 (2019) 120076.

[77] M. Osman, A. Zaabout, S. Cloete, S. Amini, Mapping the operating performance of a novel internally circulating fluidized bed reactor applied to chemical looping combustion, Fuel Process. Technol. 197 (2020) 106183.

[78] Y.-O. Chong, D.J. Nicklin, P.J. Tait, Solids exchange between adjacent fluid beds without gas mixing, Powder Technol. 47 (1986) 151–156.

[79] Y. He, V. Rudolph, Gas-solids flow in the riser of a circulating fluidized bed, in: Chem. Enoineering Sci., 1995: pp. 3443–3453.

[80] M. Fang, C. Yu, Z. Shi, Q. Wang, Z. Luo, K. Cen, Experimental research on solid circulation in a twin fluidized bed system, Chem. Eng. J. 94 (2003) 171–178.

[81] B. Kronberger, E. Johansson, G. Löffler, T. Mattisson, A. Lyngfelt, H. Hofbauer, A Two-Compartment Fluidized Bed Reactor for CO2 Capture by Chemical-Looping Combustion, Chem. Eng. Technol. 27 (2004) 1318–1326.

[82] M. Rydén, M. Johansson, A. Lyngfelt, T. Mattisson, NiO supported on Mg–ZrO2 as oxygen carrier for chemical-looping combustion and chemical-looping reforming, Energy Environ. Sci. 2 (2009) 970.

[83] E. Johansson, T. Mattisson, A. Lyngfelt, H. Thunman, A 300 W laboratory reactor system for chemical-looping combustion with particle circulation, Fuel. 85 (3AD) 1428–1438.

[84] J. Herguido, J.A. Peña, E. Carazo, Experimental assessment of hydrogen separation from H2/CH4 mixtures by the “steam-iron process” in an interconnected circulating fluidized bed reactor, Int. J. Hydrogen Energy. 39 (2014) 14050–14060.

[85] M. Osman, A. Zaabout, S. Cloete, S. Amini, Experimental demonstration of pressurized chemical looping combustion in an internally circulating reactor for power production with integrated CO2 capture, Chem. Eng. J. 401 (2020) 125974.

[86] E. Kimball, H.P. Hamers, P. Cobden, F. Gallucci, M. van S. Annaland, Operation of fixed-bed chemical looping combustion, Energy Procedia. 37 (2013) 575–579.

[87] S. Bock, R. Zacharias, V. Hacker, Co-production of pure hydrogen, carbon dioxide and nitrogen in a 10 kW fixed-bed chemical looping system, Sustain. Energy Fuels. 4 (2020) 1417–1426.

[88] S. Noorman, M. van Sint Annaland, Kuipers, Packed Bed Reactor Technology for Chemical-Looping Combustion, Ind. Eng. Chem. Res. 46 (2007) 4212–4220.

[89] S. Cloete, F. Gallucci, M. van Sint Annaland, S. Amini, Gas Switching as a Practical Alternative for Scaleup of Chemical Looping Combustion, Energy Technol. 4 (2016) 1286–1298.

[90] V. Spallina, F. Gallucci, M.C. Romano, M. Van, S. Annaland, Pre-combustion packed bed chemical looping (PCCL) technology for efficient H 2 -rich gas production processes, Chem. Eng. J. 294 (2016) 478–494.

[91] H. Jin, M. Ishida, Reactivity Study on Natural-Gas-Fueled Chemical-Looping Combustion by a Fixed-Bed Reactor, Ind. Eng. Chem. Res. 41 (2002) 4004–4007.

[92] F. Gallucci, H.P. Hamers, M. van Zanten, M. van Sint Annaland, Experimental demonstration of chemical-looping combustion of syngas in packed bed reactors with ilmenite, Chem. Eng. J. 274 (2015) 156–168.

[93] H.P. Hamers, F. Gallucci, G. Williams, M. van Sint Annaland, Experimental demonstration of CLC and the pressure effect in packed bed reactors using NiO/CaAl2O4 as oxygen carrier, Fuel. 159 (2015) 828–836.

[94] S. Nestl, G. Voitic, M. Lammer, B. Marius, J. Wagner, V. Hacker, The production of pure pressurised hydrogen by the reformer-steam iron process in a fixed bed reactor system, J. Power Sources. 280 (2015) 57–65.

[95] G. Voitic, S. Nestl, M. Lammer, J. Wagner, V. Hacker, Pressurized hydrogen production by fixed-bed chemical looping, Appl. Energy. 157 (2015) 399–407.

[96] G. Voitic, S. Nestl, K. Malli, J. Wagner, B. Bitschnau, F.-A. Mautner, V. Hacker, High purity pressurised hydrogen production from syngas by the steam-iron process, RSC Adv. 6 (2016) 53533–53541. doi:10.1039/c6ra06134f.

[97] S. Nestl, G. Voitic, R. Zacharias, S. Bock, V. Hacker, High-Purity Hydrogen Production with the Reformer Steam Iron Cycle, Energy Technol. 6 (2018) 563–569. doi:10.1002/ente.201700576.

[98] R. Zacharias, S. Visentin, S. Bock, V. Hacker, High-pressure hydrogen production with inherent sequestration of a pure carbon dioxide stream via fixed bed chemical looping, Int. J. Hydrogen Energy. 44 (2019) 7943–7957. doi:10.1016/j.ijhydene.2019.01.257.

[99] R. Xiao, Q. Song, M. Song, Z. Lu, S. Zhang, L. Shen, Pressurized chemical-looping combustion of coal with an iron ore-based oxygen carrier, Combust. Flame. 157 (2009) 1140–1153. doi:10.1016/j.combustflame.2010.01.007.

[100] R. Xiao, Q. Song, S. Zhang, W. Zheng, Y. Yang, Pressurized Chemical-Looping Combustion of Chinese Bituminous Coal: Cyclic Performance and Characterization of Iron Ore-Based Oxygen Carrier, Energy Fuels. 24 (2009) 1449–1463. doi:10.1021/ef901070c.

[101] S. Zhang, C. Saha, Y. Yang, S. Bhattacharya, R. Xiao, Use of Fe2O3-Containing Industrial Wastes As the Oxygen Carrier for Chemical-Looping Combustion of Coal:

Effects of Pressure and Cycles, 25 (2011) 4357–4366.

[102] Z. Gu, K. Li, H. Wang, S. Qing, X. Zhu, Y. Wei, X. Cheng, H. Yu, Y. Cao, Bulk monolithic Ce–Zr–Fe–O/Al 2 O 3 oxygen carriers for a fixed bed scheme of the chemical looping combustion: Reactivity of oxygen carrier, Appl. Energy. 163 (2016) 19–31.

[103] H. Zhang, X. Liu, H. Hong, H. Jin, Characteristics of a 10 kW honeycomb reactor for natural gas fueled chemical-looping combustion, Appl. Energy. 213 (2018) 285–292.

[104] H. Zhang, H. Hong, Q. Jiang, Y. Deng, H. Jin, Q. Kang, Development of a chemical-looping combustion reactor having porous honeycomb chamber and experimental validation by using NiO/NiAl2O4, Appl. Energy. 211 (2018) 259–268.

[105] D. Sridhar, A. Tong, H. Kim, L. Zeng, F. Li, L.-S. Fan, Syngas Chemical Looping Process: Design and Construction of a 25 kW th Subpilot Unit, Energy & Fuels. 26 (2012) 2292–2302.

[106] P. Gupta, L.G. Velazquez-Vargas, L.-S. Fan, Syngas Redox (SGR) Process to Produce Hydrogen from Coal Derived Syngas, Energy & Fuels. 21 (2007) 2900–2908.

[107] F. Li, L. Zeng, L.G. Velazquez-Vargas, Z. Yoscovits, L.-S. Fan, Syngas chemical looping gasification process: Bench-scale studies and reactor simulations, AIChE J. 56 (2010) 2186–2199.

[108] A. Tong, D. Sridhar, Z. Sun, H.R. Kim, L. Zeng, F. Wang, D. Wang, M. V. Kathe, S. Luo, Y. Sun, L.-S. Fan, Continuous high purity hydrogen generation from a syngas chemical looping 25 kWth sub-pilot unit with 100% carbon capture, Fuel. 103 (2013) 495–505.

[109] T.-L. Hsieh, D. Xu, Y. Zhang, S. Nadgouda, D. Wang, C. Chung, Y. Pottimurphy, M. Guo, Y.-Y. Chen, M. Xu, P. He, L.-S. Fan, A. Tong, 250 kWth high pressure pilot demonstration of the syngas chemical looping system for high purity H2 production with CO2 capture, Appl. Energy. 230 (2018) 1660–1672.

[110] I.M. Dahl, E. Bakken, Y. Larring, A.I. Spjelkavik, S.F. Håkonsen, R. Blom, On the development of novel reactor concepts for chemical looping combustion, Energy Procedia. 1 (2009) 1513–1519.

[111] Z. Zhao, T. Chen, A.F. Ghoniem, Rotary Bed Reactor for Chemical-Looping Combustion with Carbon Capture. Part 1: Reactor Design and Model Development, Energy Fuels. 27 (2013) 327−343.

[112] S.F. Håkonsen, R. Blom, Chemical Looping Combustion in a Rotating Bed Reactor – Finding Optimal Process Conditions for Prototype Reactor, Environ. Sci. Technol. 45 (2011) 9619–9626.

[113] S.F. Håkonsen, C.A. Grande, R. Blom, Rotating bed reactor for CLC: Bed characteristics dependencies on internal gas mixing, Appl. Energy. 113 (2014) 1952–1957.

[114] Z. Zhao, T. Chen, A.F. Ghoniem, Rotary Bed Reactor for Chemical-Looping Combustion with Carbon Capture. Part 2: Base Case and Sensitivity Analysis, Energy Fuels. 27 (2013) 344−359.

[115] Z. Zhao, C.O. Iloeje, T. Chen, A.F. Ghoniem, Design of a rotary reactor for chemical-

looping combustion. Part 1: Fundamentals and design methodology, Fuel. 121 (2014) 327–343.

[116] Z. Zhao, A.F. Ghoniem, Design of a rotary reactor for chemical-looping combustion. Part 2: Comparison of copper-, nickel-, and iron-based oxygen carriers, Fuel. 121 (2014) 344–360.

[117] C. Iloeje, Z. Zhao, A.F. Ghoniem, Efficient cycles for carbon capture CLC power plants based on thermally balanced redox reactors, Int. J. Greenh. Gas Control. 41 (2015) 302–315.

[118] C.O. Iloeje, Z. Zhao, A.F. Ghoniem, A reduced fidelity model for the rotary chemical looping combustion reactor, Appl. Energy. 190 (2017) 725–739.

[119] C.O. Iloeje, Z. Zhao, A.F. Ghoniem, Design and techno-economic optimization of a rotary chemical looping combustion power plant with CO2 capture, Appl. Energy. 231 (2018) 1179–1190.

[120] O.V. Ogidiama, M. Abu Zahra, T. Shamim, Techno-Economic Analysis of a Carbon Capture Chemical Looping Combustion Power Plant, J. Energy Resour. Technol. 140 (2018) 112004.

[121] L. Zhu, Y. He, L. Li, P. Wu, Tech-economic assessment of second-generation CCS: Chemical looping combustion, Energy. 144 (2018) 915–927.

[122] R. Porrazzo, G. White, R. Ocone, Techno-economic investigation of a chemical looping combustion based power plant, Faraday Discuss. 192 (2016) 437–457.

[123] O.V. Ogidiama, M.R.M. Abu-Zahra, T. Shamim, Techno-economic analysis of a poly-generation solar-assisted chemical looping combustion power plant, Appl. Energy. 228 (2018) 724–735.

[124] G. Diglio, P. Bareschino, E. Mancusi, F. Pepe, Techno-Economic Evaluation of a Small-Scale Power Generation Unit Based on a Chemical Looping Combustion Process in Fixed Bed Reactor Network, Ind. Eng. Chem. Res. 57 (2018) 11299–11311.

[125] C.O. Iloeje, Z. Zhao, A.F. Ghoniem, Design and techno-economic optimization of a rotary chemical looping combustion power plant with CO2 capture, Appl. Energy. 231 (2018) 1179–1190.

[126] M.N. Khan, P. Chiesa, S. Cloete, S. Amini, Integration of chemical looping combustion for cost-effective CO2 capture from state-of-the-art natural gas combined cycles, Energy Convers. Manag. X. (2020) 100044.

[127] L. Mancuso, S. Cloete, P. Chiesa, S. Amini, Economic assessment of packed bed chemical looping combustion and suitable benchmarks, Int. J. Greenh. Gas Control. 64 (2017) 223–233.

[128] S. Cloete, A. Tobiesen, J. Morud, M. Romano, P. Chiesa, A. Giuffrida, Y. Larring, Economic assessment of chemical looping oxygen production and chemical looping combustion in integrated gasification combined cycles, Int. J. Greenh. Gas Control. 78 (2018) 354–363.

[129] A. Farooqui, A. Bose, D. Ferrero, J. Llorca, M. Santarelli, Techno-economic and exergetic assessment of an oxy-fuel power plant fueled by syngas produced by chemical looping CO2 and H2O dissociation, J. CO2 Util. 27 (2018) 500–517.

[130] S.M. Nazir, J.F. Morgado, O. Bolland, R. Quinta-Ferreira, S. Amini, Techno-economic assessment of chemical looping reforming of natural gas for hydrogen production and power generation with integrated CO2 capture, Int. J. Greenh. Gas Control. 78 (2018) 7–20.

[131] S.M. Nazir, S. Cloete, O. Bolland, S. Amini, Techno-economic assessment of the novel gas switching reforming (GSR) concept for gas-fired power production with integrated CO2 capture, Int. J. Hydrogen Energy. 43 (2018) 8754–8769.

[132] S.M. Nazir, J.H. Cloete, S. Cloete, S. Amini, Pathways to low-cost clean hydrogen production with gas switching reforming, Int. J. Hydrogen Energy. (2020).

[133] S.A. Wassie, S. Cloete, V. Spallina, F. Gallucci, S. Amini, M. van Sint Annaland, Techno-economic assessment of membrane-assisted gas switching reforming for pure H2 production with CO2 capture, Int. J. Greenh. Gas Control. 72 (2018) 163–174.

[134] V. Spallina, D. Pandolfo, A. Battistella, M.C. Romano, M. Van, S. Annaland, F. Gallucci, Techno-economic assessment of membrane assisted fluidized bed reactors for pure H2 production with CO2 capture, Energy Convers. Manag. 120 (2016) 257–273.

[135] V. Spallina, A. Shams, A. Battistella, F. Gallucci, M.V.S. Annaland, Chemical Looping Technologies for H2 Production with CO2 Capture: Thermodynamic Assessment and Economic Comparison, in: Energy Procedia, Elsevier Ltd, 2017: pp. 419–428.

[136] S. Cloete, M.N. Khan, S. Amini, Economic assessment of membrane-assisted autothermal reforming for cost effective hydrogen production with CO2 capture, Int. J. Hydrogen Energy. 44 (2019) 3492–3510.

[137] M.N. Khan, T. Shamim, Techno-economic assessment of a plant based on a three reactor chemical looping reforming system, Int. J. Hydrogen Energy. 41 (2016) 22677–22688.

[138] M.N. Khan, T. Shamim, Techno-economic assessment of a chemical looping reforming combined cycle plant with iron and tungsten based oxygen carriers, Int. J. Hydrogen Energy. 44 (2019) 11525–11534.

[139] D.A. Chisalita, C.C. Cormos, Techno-economic assessment of hydrogen production processes based on various natural gas chemical looping systems with carbon capture, Energy. 181 (2019) 331–344.

[140] D. Xiang, Y. Zhou, Concept design and techno-economic performance of hydrogen and ammonia co-generation by coke-oven gas-pressure swing adsorption integrated with chemical looping hydrogen process, Appl. Energy. 229 (2018) 1024–1034.

[141] L. Zhu, Y. He, L. Li, P. Wu, Tech-economic assessment of second-generation CCS: Chemical looping combustion, Energy. 144 (2018) 915–927.

[142] F. Zerobin, S. Penthor, O. Bertsch, T. Pröll, Fluidized bed reactor design study for pressurized chemical looping combustion of natural gas, Powder Technol. 316 (2017) 569–577.

[143] V. Spallina, M.C. Romano, P. Chiesa, F. Gallucci, M. Van, S. Annaland, G. Lozza, Integration of coal gasification and packed bed CLC for high efficiency and near-zero emission power generation, Int. J. Greenh. Gas Control. 27 (2014) 28–41.

[144] C. Arnaiz del Pozo, S. Cloete, J.H. Cloete, Á. Jiménez Álvaro, S. Amini, The potential of chemical looping combustion using the gas switching concept to eliminate the energy

penalty of CO2 capture, Int. J. Greenh. Gas Control. 83 (2019) 265–281.

[145] C. Pozo, J. Cloete, S. Cloete, Á. Álvaro, S. Amini, Integration of Gas Switching Combustion in a Humid Air Turbine cycle for flexible power production from solid fuels with near-zero emissions, Int. J. Energy Res. (2020).

[146] A. Zaabout, S. Cloete, S.T. Johansen, M. van Sint Annaland, F. Gallucci, S. Amini, Experimental Demonstration of a Novel Gas Switching Combustion Reactor for Power Production with Integrated CO2 Capture, Ind. Eng. Chem. Res. 52 (2013) 14241–14250.

[147] S.M. Nazir, J.H. Cloete, S. Cloete, S. Amini, Gas switching reforming (GSR) for power generation with CO2 capture: Process efficiency improvement studies, Energy. 167 (2019) 757–765.

[148] S. Szima, S.M. Nazir, S. Cloete, S. Amini, S. Fogarasi, A.-M. Cormos, C.-C. Cormos, Gas switching reforming for flexible power and hydrogen production to balance variable renewables, Renew. Sustain. Energy Rev. 110 (2019) 207–219.

[149] S. Cloete, L. Hirth, Flexible power and hydrogen production: Finding synergy between CCS and variable renewables, Energy. 192 (2020) 116671.

[150] C. Arnaiz del Pozo, S. Cloete, P. Chiesa, Á. Jiménez Álvaro, S. Amini, Integration of gas switching combustion and membrane reactors for exceeding 50% efficiency in flexible IGCC plants with near-zero CO2 emissions, Energy Convers. Manag. X. 7 (2020) 100050.

[151] S.M. Nazir, J.H. Cloete, S. Cloete, S. Amini, Efficient hydrogen production with CO2 capture using gas switching reforming, Energy. 185 (2019) 372–385.

[152] S. Cloete, M.N. Khan, S.M. Nazir, S. Amini, Cost-effective clean ammonia production using membrane-assisted autothermal reforming, Chem. Eng. J. 404 (2021) 126550.

[153] R.J. Lee Pereira, P.A. Argyris, V. Spallina, A comparative study on clean ammonia production using chemical looping based technology, Appl. Energy. 280 (2020) 115874.

[154] V. Spallina, G. Motamedi, F. Gallucci, M. van Sint Annaland, Techno-economic assessment of an integrated high pressure chemical-looping process with packed-bed reactors in large scale hydrogen and methanol production, Int. J. Greenh. Gas Control. 88 (2019) 71–84.

[155] J.C. Abanades, B. Arias, A. Lyngfelt, T. Mattisson, D.E. Wiley, H. Li, M.T. Ho, E. Mangano, S. Brandani, Emerging CO2 capture systems, Int. J. Greenh. Gas Control. 40 (2015) 126–166.

[156] D.P. Harrison, Sorption-Enhanced Hydrogen Production: A Review, Ind. Eng. Chem. Res. 47 (2008) 6486–6501.

[157] E.J. Ben Anthony, Ca looping technology: current status, developments and future directions, Greenh. Gases Sci. Technol. 1 (2011) 36–47.

[158] J.W. Butler, J.R. Grace, High-pressure systems and processes for calcium looping, in: Calcium Chem. Looping Technol. Power Gener. Carbon Dioxide Capture, Woodhead Publishing, 2015: pp. 377–408.

[159] Q. Wang, N. Rong, H. Fan, Y. Meng, M. Fang, L. Cheng, K. Cen, Enhanced hydrogen-rich gas production from steam gasification of coal in a pressurized fluidized bed with

CaO as a CO2 sorbent, Int. J. Hydrogen Energy. 39 (2014) 5781–5792.

[160] J.G. Yao, M.E. Boot-Handford, Z. Zhang, G.C. Maitland, P.S. Fennell, Pressurized in Situ CO2 Capture from Biomass Combustion via the Calcium Looping Process in a Spout-Fluidized-Bed Reactor, Ind. Eng. Chem. Res. 59 (2020) 8571–8580.

[161] A. Obradović, J. Levec, High Purity Hydrogen with Sorption-Enhanced Steam Methane Reforming in a Gas–Solid Trickle Bed Reactor, Ind. Eng. Chem. Res. 56 (2017) 13301–13309.

[162] Y. Fan, J.G. Yao, Z. Zhang, M. Sceats, Y. Zhuo, L. Li, G.C. Maitland, P.S. Fennell, Pressurized calcium looping in the presence of steam in a spout-fluidized-bed reactor with DFT analysis, Fuel Process. Technol. 169 (2018) 24–41.

[163] X. Zhou, X. Yang, J. Li, J. Zhao, C. Li, M. Du, Z. Yu, Y. Fang, Pressurized catalytic calcium looping hydrogen generation from coal with in-situ CO2 capture, Energy Convers. Manag. 198 (2019) 111899.

[164] I. Martínez, M. Martini, L. Riva, F. Gallucci, M. Van Sint Annaland, M.C. Romano, Techno-economic analysis of a natural gas combined cycle integrated with a Ca-Cu looping process for low CO2 emission power production, Int. J. Greenh. Gas Control. 81 (2019) 216–239.

[165] J.R. Fernández, J.M. Alarcón, J.C. Abanades, Study of the calcination of CaCO3 by means of a Cu/CuO chemical loop using methane as fuel gas, Catal. Today. 333 (2019) 176–181.

[166] L. Díez-Martín, J.M. López, I. Martínez, G. Grasa, R. Murillo, J.R. Fernández, Experimental investigation of the Ca-Cu process for H2 production: Evaluation of reduction/calcination strategies, Int. J. Greenh. Gas Control. 83 (2019) 43–50.

[167] V. Manovic, E.J. Anthony, Integration of calcium and chemical looping combustion using composite CaO/CuO-based materials, Environ. Sci. Technol. 45 (2011) 10750–10756.

[168] J.R. Fernández, J.C. Abanades, Overview of the Ca–Cu looping process for hydrogen production and/or power generation, Curr. Opin. Chem. Eng. 17 (2017) 1–8.

[169] Y. Hu, H. Cui, Z. Cheng, Z. Zhou, Sorption-enhanced water gas shift reaction by in situ CO2 capture on an alkali metal salt-promoted MgO-CaCO3 sorbent, Chem. Eng. J. 377 (2019) 119823.

[170] M.A. Soria, C. Rocha, S. Tosti, A. Mendes, L.M. Madeira, COx free hydrogen production through water-gas shift reaction in different hybrid multifunctional reactors, Chem. Eng. J. 356 (2019) 727–736.